

# Resolving the energy alignment between methylammonium lead iodide and C<sub>60</sub>: an in-situ photoelectron spectroscopy study

Alberto García-Fernández<sup>a,b##</sup>, Karen Radetzky<sup>a,c#</sup>, Stefania Riva<sup>a</sup>, Birgit Kammlander<sup>a</sup>, Brian Rydgren<sup>a,c</sup>, Evelyn Johannesson<sup>a,c</sup>, Rahul Mahavir Varma<sup>a</sup>, Håkan Rensmo<sup>a,c</sup>, Ute B. Cappel<sup>a,c\*</sup>

Understanding and controlling the energy level alignment at interfaces between lead halide perovskites and electron transport layers is crucial for optimizing charge extraction by minimizing recombination losses in high-efficiency perovskite solar cells. In this work, we investigated the energy level alignment of C<sub>60</sub> on in-situ cleaved MAPbI<sub>3</sub> single crystals in multiple repeat experiments using photoelectron spectroscopy aiming to resolve inconsistencies reported in earlier studies. Our results show that both materials remain chemically stable upon interface formation, the strong reactions typically seen when metals contact perovskites. By analyzing Pb 4f and C 1s core level positions in detail, we determined that C<sub>60</sub> consistently exhibits a downward energy shift toward MAPbI<sub>3</sub>, which works against efficient charge extraction. The magnitude of this shift, however, is highly sensitive to the surface composition, highlighting that small variations may lead to significant differences in results. At higher C<sub>60</sub> coverages of more than 5 monolayers, a constant HOMO–valence band offset of 0.52 eV was obtained. Assuming a 1.86 eV HOMO–LUMO gap, the C<sub>60</sub> LUMO is 0.25 eV below the MAPbI<sub>3</sub> conduction band, a value favorable for charge extraction. These findings underscore the decisive role of surface chemistry on interfacial energetics, explain performance variability in perovskite devices, and demonstrate the need to control and accurately measure surface properties. Furthermore, the observed energetic alignment can explain why further interface modification by charge blocking layers or surface passivation is needed for optimized device efficiencies.

## Introduction

In the development of sustainable energy harvesting technologies, perovskite solar cells (PSCs) are a popular candidate. Highly efficient PSCs are based on organic-inorganic metal halide absorber materials.<sup>1</sup> Besides desirable optoelectronic properties such as long carrier diffusion lengths and lifetimes, compositional engineering allows for tuning the material's band gap.<sup>2</sup> Moreover, PSCs are an example of a thin film technology wherein it is possible to fabricate many layers via solution processing.<sup>3</sup> Research in efficiency and stability is progressing along several avenues distinguished by the solar cell architecture, which is divided into n-i-p or p-i-n single junction and multi junction devices. A commonality across these technologies is the need for efficient charge extraction from the perovskite with subsequent charge transport to the contacts.<sup>4</sup> This is achieved by placing the absorber between an electron transport layer (ETL) and a hole transport layer (HTL). The materials are chosen to facilitate selective charge extraction due to the energetic gradient and alignment at the interfaces – with electrons being transferred from the perovskite to the ETL. Many well established ETLs are based on a fullerene motif.<sup>5</sup> In p-i-n devices, functionalized C<sub>60</sub> and its derivatives are typically employed to tailor the solubility, electronic properties, and interface interactions. For example, PCBM is prevalently used as

the ETL in p-i-n devices.<sup>6,7</sup> These devices achieve efficiencies of up to 26%.<sup>8</sup> Moreover, Elnaggar et al. have presented two further fullerene ETLs which improved stability under aging conditions in MAPbI<sub>3</sub> based p-i-n devices.<sup>9</sup> Additionally, unaltered C<sub>60</sub> is also used in photovoltaic devices and has been demonstrated to be beneficial to long-term stability in p-i-n devices based on Cs<sub>0.175</sub>FA<sub>0.750</sub>MA<sub>0.075</sub>Pb(I<sub>0.880</sub>Br<sub>0.120</sub>)<sub>3</sub>.<sup>10,11</sup> Momblona et al. demonstrate p-i-n and n-i-p devices employing C<sub>60</sub> to contact a MAPbI<sub>3</sub> absorber with suppressed hysteresis.<sup>12</sup> Yet, it has often been found that passivation of the perovskite and/or additional charge blocking layers (e.g. LiF, BCP) are needed for the best device performance.<sup>13–16</sup>

Despite upcoming new approaches, C<sub>60</sub> layers are commonly fabricated via thermal evaporation.<sup>17</sup> This is advantageous for the assembly of multijunction solar cells, where the deposition parameters of top layers such as solvents and temperature are constricted by the stability of the underlying stack. C<sub>60</sub> layers are thus also widely applied as an ETL in multijunction perovskite solar cells.<sup>18</sup> Hu et al. utilized C<sub>60</sub> in double, triple, and quadrupole junction solar cells in contact with mixed cation lead halide perovskites Cs<sub>0.1</sub>FA<sub>0.9</sub>Pb(I<sub>0.85</sub>Br<sub>0.15</sub>)<sub>3</sub> and Cs<sub>0.05</sub>FA<sub>0.90</sub>MA<sub>0.05</sub>PbI<sub>2.95</sub>Br<sub>0.05</sub> and achieved devices with 28.2%, 28.0%, and 26.9% power conversion efficiency, respectively.<sup>19</sup>

Due to this widespread application, understanding the energetic alignment of C<sub>60</sub> to the perovskite is of great importance to fully comprehend device performance and limitations.<sup>20–22</sup> Ideally, the LUMO of C<sub>60</sub> should be below the perovskite conduction band to enable electron transfer. Furthermore, upward energy level shifts (often referred to as band bending) in the C<sub>60</sub> towards the perovskite would facilitate electron movement away from interface and be beneficial for charge extraction. MAPbI<sub>3</sub> is simultaneously a popular perovskite and the first for which a heterojunction with C<sub>60</sub> was

<sup>a</sup> Division of X-ray Photon Science, Department of Physics and Astronomy, Uppsala University, Box 516, SE-751 20, Uppsala, Sweden. E-mail: ute.cappel@physics.uu.se

<sup>b</sup> Universidade da Coruña, CICA (Interdisciplinary Center for Chemistry and Biology), Department of Chemistry, Faculty of Science, As Carballeiras, s/n, Campus de Elviña 15071 A Coruña, Spain. E-mail: alberto.garcia.fernandez@udc.es

<sup>c</sup> Wallenberg Initiative Materials Science for Sustainability, Department of Physics and Astronomy, Uppsala University, 751 20 Uppsala, Sweden

# The authors contributed equally to the work.

reported.<sup>23</sup> Therefore, numerous studies have already investigated the energetic alignment between  $\text{MAPbI}_3$  and  $\text{C}_{60}$ , however, without reaching a consensus on the energetics of the interface.

Schulz et al. explored  $\text{C}_{60}$  layers of increasing thickness on a  $\text{MAPbI}_3$  thin film substrate with photoelectron spectroscopy and found close alignment of the  $\text{C}_{60}$  LUMO and the perovskite conduction band.<sup>24</sup> However, Lo et al. reported the band gap of  $\text{MAPbI}_3$  to be within the  $\text{C}_{60}$  band gap forming a n-n junction and place the  $\text{C}_{60}$  LUMO significantly above the perovskite conduction band.<sup>25</sup> A publication by Wang et al. presents a band model with significant upwards band bending towards the interface in the underlying perovskite and downwards band bending in  $\text{C}_{60}$ .<sup>26</sup> This band alignment would be unsuitable for electron extraction from the perovskite to  $\text{C}_{60}$ , even though the  $\text{C}_{60}$  LUMO is found to be energetically below the  $\text{MAPbI}_3$  conduction band in their study. For two step perovskite thin film preparation, Shin et al. determined that the energetic alignment to  $\text{C}_{60}$  depends on the concentration of MAI used in the second step and relate this to the extent of conversion to  $\text{MAPbI}_3$  and p-doping with excess MAI.<sup>27</sup> Lastly, Quarti et al. presented a theoretical study emphasizing that the surface termination of the  $\text{MAPbI}_3$  perovskite critically determines the alignment to the  $\text{C}_{60}$  orbitals and show that beneficial alignment is only present for MAI terminated surfaces.<sup>28</sup> Furthermore, these previous reports show significant differences between the work functions determined for  $\text{MAPbI}_3$  and for the  $\text{C}_{60}$ , which may depend on the substrate of the perovskite and on differences in sample and surface compositions. These varying reports serve to highlight that the energetic alignment between  $\text{MAPbI}_3$  and  $\text{C}_{60}$  is still not fully understood.

Within the study here presented, the energetic alignment between thermally evaporated  $\text{C}_{60}$  layers and in-situ cleaved  $\text{MAPbI}_3$  single crystal surfaces is explored for the first time using synchrotron-based soft X-ray photoelectron spectroscopy (PES). As the cleaved single crystal surface is almost free from adsorbates, contaminants, and grain boundaries, we thus base our investigation on a well-defined, clean sample system, in contrast to previous studies. Furthermore, due to the bulk thickness of the single crystal, the results are not influenced by a substrate below the perovskite. Additionally, we perform a series of duplicate experiments, to be able to study variations in the energy alignment at the perovskite/ $\text{C}_{60}$  interface. To be able to compare the different experiments, we use relative core level positions: The analysis is based on the energy difference between the Pb 4f and C 1s core level peaks, which are characteristic to  $\text{MAPbI}_3$  and  $\text{C}_{60}$ , respectively, and can be very accurately determined. This allows for the determination of the energy offset between the two materials and an easy and reliable comparison between different experiments. While we find variations in the energy alignment between different experiments, we find a general trend of a downwards energy shift in the  $\text{C}_{60}$  layer towards the perovskite and a constant energy offset between the perovskite bands and  $\text{C}_{60}$  orbitals for thicker  $\text{C}_{60}$  layers.

## Methods

### Single crystal synthesis

Methylammonium lead iodide ( $\text{MAPbI}_3$ ) single crystals of approximately 0.5 cm diameter were obtained by inverse temperature crystallization and following the methodology described in our previous publication.<sup>29</sup> In summary, a 1M solution in  $\gamma$ -butyrolactone (GBL) of MAI ( $\text{CH}_3\text{NH}_3\text{I}$ ) (Sigma-Aldrich) and  $\text{PbI}_2$  (TCI) (1:1) was prepared by stirring at room temperature. Once completely dissolved, the solution was filtered through a 0.45  $\mu\text{m}$  PTFE filter and heated up to 100 °C. After 3 h, selected crystals were collected.

### Photoelectron spectroscopy measurements

PES was carried out during three different beamtimes at the FlexPES beamline at MAX IV.<sup>30</sup> The X-rays from the undulator source were monochromatized using a plane grating monochromator (modified Zeiss SX700). The exit slit was adjusted to reduce the X-ray flux on the sample. Typically, an exit slit of 10  $\mu\text{m}$  was used for a photon energy of 535 eV and either 5 or 10  $\mu\text{m}$  was used for 130 and 758 eV. The endstation employs a Scienta DA30-L(W) spectrometer with a 40 mm MCP/CCD detector. The spectrometer slit was set to 500  $\mu\text{m}$  and a pass energy of 100 eV was used. With these settings and a beamline slit of 10  $\mu\text{m}$ , the combined energy resolution of the spectrometer and the X-rays is 139 meV at 130 eV, 146 meV at 535 eV and 157 meV at 758 eV. The measurement chamber was under ultra-high vacuum conditions with a pressure of  $1 \times 10^{-9}$  to  $1 \times 10^{-10}$  mbar.

Single crystals were mounted on sample plates using two-component conductive epoxy EPO-TEK H20E. The epoxy was cured at 100 °C for 1 h. Clean single crystal surfaces were achieved by blade cleaving under high-vacuum conditions. After initial characterization of the perovskite surface,  $\text{C}_{60}$  layers were deposited via thermal evaporation from a molecular source (Sigma Aldrich). The samples were characterized before and after each evaporation by core level measurements with different photon energies (535 and 758 eV) and valence band measurements with 130 and 535 eV. For each single crystal, one main spot and at least one control spot were measured.

Within this study, data from three different  $\text{MAPbI}_3$  single crystals measured on three different beamtimes will be shown and named as: Exp 1 (Data from January 2023), Exp 2 (Data from December 2023), and Exp 3 (Data from September 2024). In addition to measuring all core levels at different photon energies in one spot on the sample (Spot 1), we also measured C 1s and Pb 4f core levels with a photon energy of 535 eV in a different spot (named Spot 2) on the same single crystal and beamtime. As only two core levels were measured, this leads to a reduced X-ray exposure in this spot. Furthermore, during the third experiment, measurements with different X-ray flux densities were carried out by varying the size of the exit slit (Exp 3, Spot 3). Au 4f core level spectra were measured on a gold foil mounted on the sample plate. All core level spectra were energy calibrated by setting the position of Au 4f<sub>7/2</sub> to 84.00 eV.

## Data analysis

Photoelectron core level spectra were fitted with a Pseudo-Voigt function and a Shirley or linear background. The  $C_{60}$  coverage and thickness in number of monolayers (ML, 0.7 nm) was calculated based on the peak attenuation of the Pb 4f photoelectron peak and the electron inelastic mean free path ( $\lambda$ ).<sup>31</sup>

The inelastic mean free path of electrons in  $C_{60}$  was calculated based on the TPP-2M model.<sup>32</sup> All used parameters can be found in Table S1. The  $C_{60}$  thickness in number of monolayers was calculated based on a model which assumes layer-by-layer deposition of  $C_{60}$  (Model 1, Fig S1) and is compared to a simpler one, where a layer of uniform thickness is assumed (Model 2, Fig S2). Both models give comparable results (Fig S3) when the coverage exceeds one monolayer, but Model 1 is expected to be more accurate for coverages below one monolayer and is therefore used when describing the thickness of the evaporated layers. Furthermore, the accuracy of the models is investigated by comparing values calculated with two different photon energies (Fig S4) giving an error in the estimation of about 30%.

## Results and discussion

### Core level spectra of $\text{MAPbI}_3$ surfaces

Fig 1 shows the core level spectra obtained with a photon energy of 535 eV for surfaces of three different  $\text{MAPbI}_3$  single crystals. To facilitate comparison, all spectra were energy calibrated to the same Pb 4f<sub>7/2</sub> position of 138.54 eV and normalized to the intensity of the respective Pb 4f core level.<sup>29</sup> Data recorded with a photon energy of 758 eV is shown in Fig S5. The core levels shown represent the different expected components of the  $\text{MAPbI}_3$  structure, N 1s and C 1s for methylammonium, Pb 4f for  $\text{Pb}^{2+}$ , and I 4d for I. In all experiments, the shape and intensity of the perovskite core levels are very similar, with some small variations in the nitrogen and iodine intensities in Exp 2. In accordance with our previous study, we fitted the C 1s spectrum with two contributions for methylammonium – a surface component at higher binding energies and a bulk component at lower binding energies (Fig S6).<sup>29</sup> The ratios between these two components indicate that the surfaces are mostly, but not fully, terminated by MA (more than 70% MA termination). An additional component was included at approximately 285 eV binding energy to model small amounts of adventitious carbon on the

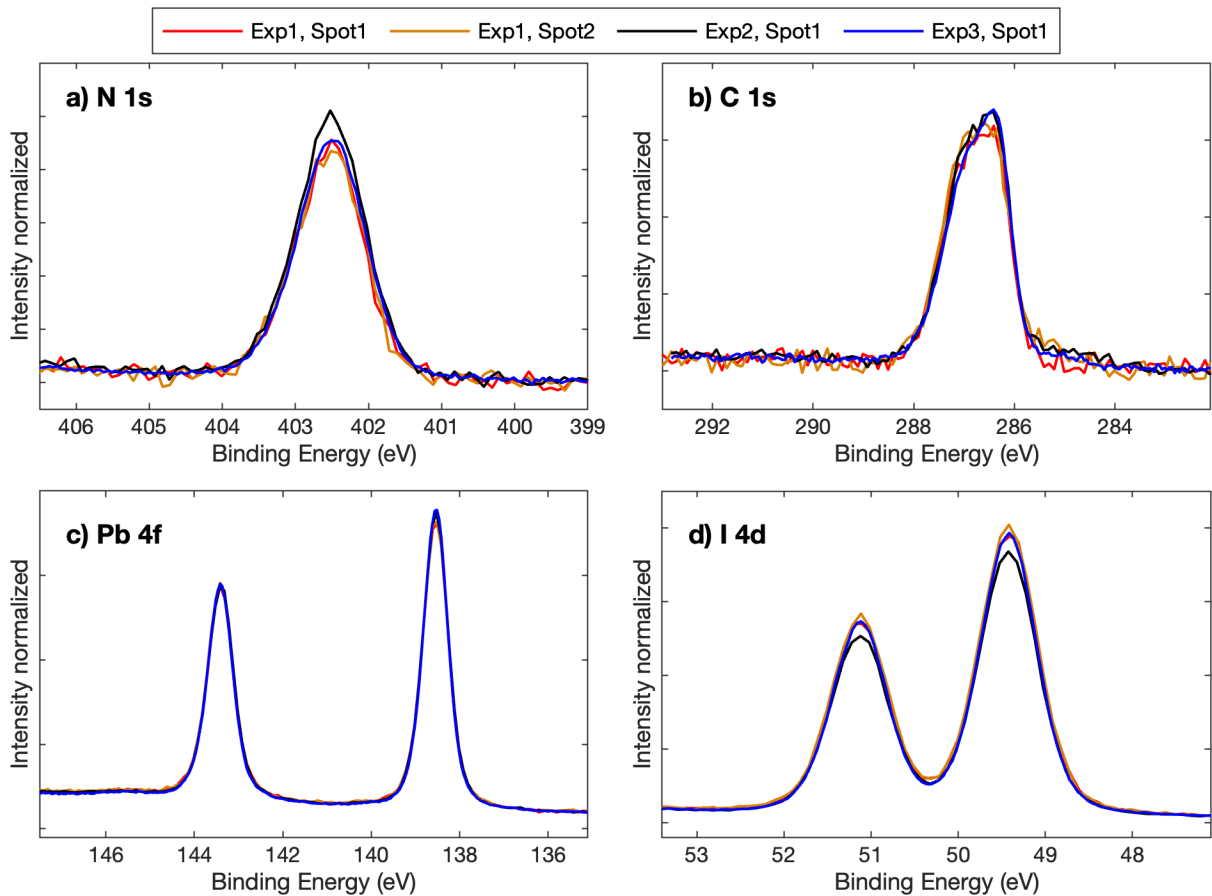


**Fig 1.** Normalized core level spectra of a) N 1s, b) C 1s, c) Pb 4f, d) I 4d of  $\text{MAPbI}_3$  single crystal surface after cleaving recorded with a photon energy of 535 eV. Data for three different single crystals measured on three different occasions (Exp 1, Exp 2 and Exp 3) and two different measurements spots (Exp 1) on one of the single crystals (Spot 1, Spot 2) is shown. The binding energy scale is calibrated by setting the Pb 4f<sub>7/2</sub> position to 138.54 eV and the intensities are normalized to the Pb 4f intensity.<sup>29</sup>

surface, which are found in all spectra except for the one obtained for spot 1 in Exp 1.

#### Core level spectra after $C_{60}$ evaporation

Following  $MAPbI_3$  surface characterization,  $C_{60}$  was evaporated in consecutive steps, and the new surface/interface was characterized by PES between each evaporation. Fig 2 shows the measured core level spectra recorded with a photon energy of 535 eV for Exp 1 (spot 1), while Fig 3 shows the same spectra calibrated and normalized to the Pb 4f core level. The same trends as described below were observed at an additional photon energy (758 eV), on another sample spot and for the two other evaporation experiments (Fig S7-S15). Additionally, valence band spectra recorded with a photon energy of 130 eV in Exp 1 are shown in Fig S16. From Fig 2, it can be seen that the intensities of the core levels associated only with the perovskite (N 1s, Pb 4f and I 4d) decrease in intensity. In the C 1s spectra, a new peak appears at approximately 285 eV which increases with consecutive evaporation and is therefore associated with  $C_{60}$  deposited on the perovskite surface. As discussed in the SI, the thickness in monolayers of the deposited  $C_{60}$  was calculated from the attenuation of the Pb 4f signal compared to the pure perovskite surface. The calculated values show some variation between different photon energies (see Fig S4) and sample spots. The latter could be due to a difference in distance/position relative to the evaporation source. In the

Figures below and in the SI, the legend states the values calculated for the respective sample spot with the same photon energy as the shown data.

The normalized spectra in Fig 3 show the impact of the evaporation on the perovskite. It can be observed that the relative intensity and shape of the perovskite components remain very similar upon all repeated evaporation. This confirms that the perovskite surface remains intact upon evaporation of  $C_{60}$ . This is in contrast to the evaporation of metals onto a perovskite surface, which can cause damage to the perovskite.<sup>33,34</sup> Fig 3b focuses on the smaller features at binding energies higher than the main  $C_{60}$  peak in the C 1s core level. Initially, the  $MA^+$  carbon is observed in a binding energy range between 286 and 288 eV. However, additional features are observed, which increase in intensity relative to the perovskite with increased number of  $C_{60}$  evaporation. These features are most clear after the final evaporation (2.9 ML) and can be assigned to  $C_{60}$  shake-up satellite peaks, which are expected at +1.8, +3.7, +4.8 and +5.9 eV higher binding energies than the main  $C_{60}$  peak.<sup>35-37</sup> In Fig 4a, we use the C 1s spectra to compare the shape of the  $C_{60}$  spectra after different evaporation. This is enabled by normalizing to the intensity and energy aligning to the position of the main  $C_{60}$  peak. It can be observed that the main  $C_{60}$  peak is slightly broadened at lower coverage. However, a magnification of the satellite region

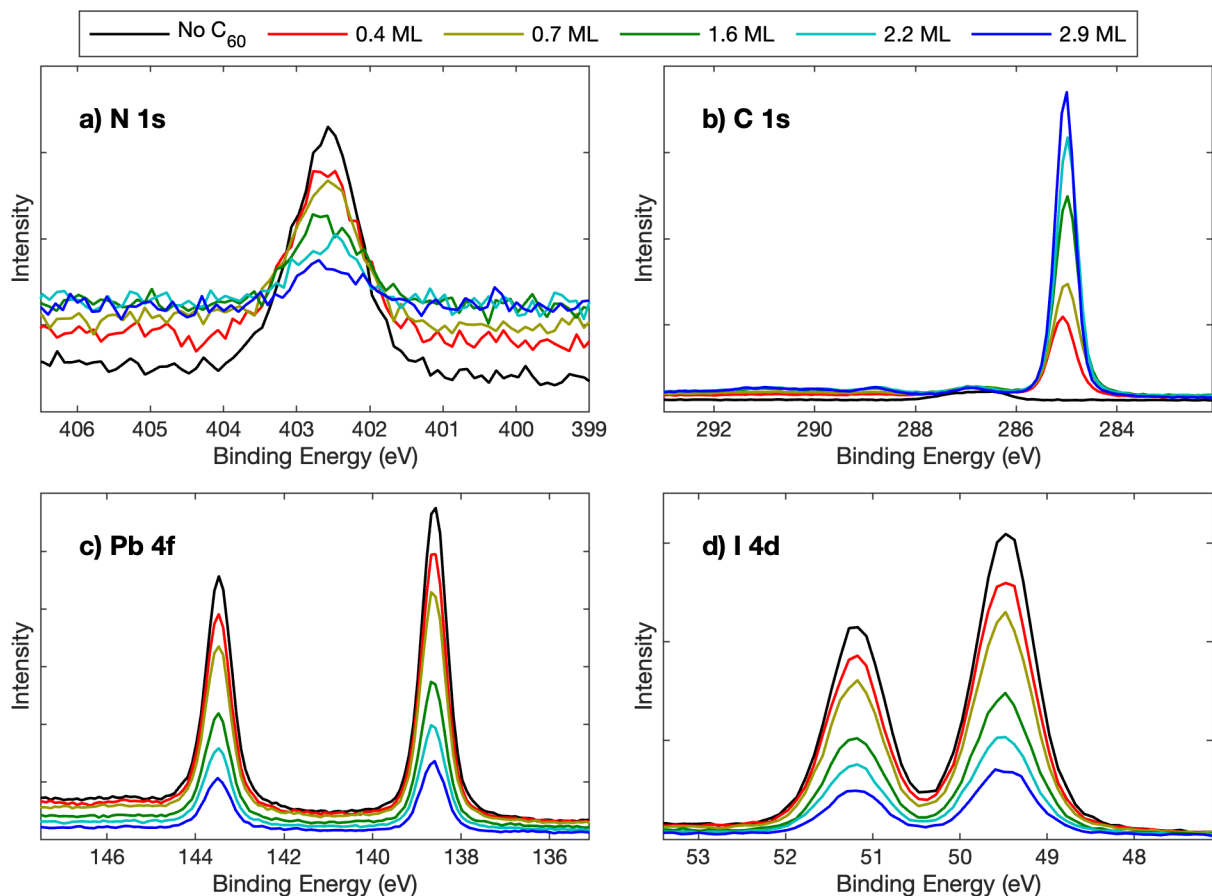


**Fig 2.** Core level spectra of a) N 1s, b) C 1s, c) Pb 4f, d) I 4d of a  $MAPbI_3$  single crystal surface in Exp 1, spot 1 after cleaving and after consecutive evaporation of  $C_{60}$  recorded with a photon energy of 535 eV. The binding energy scale is calibrated to the Fermi level through measurements of the Au 4f core level and the intensities are plotted as measured.

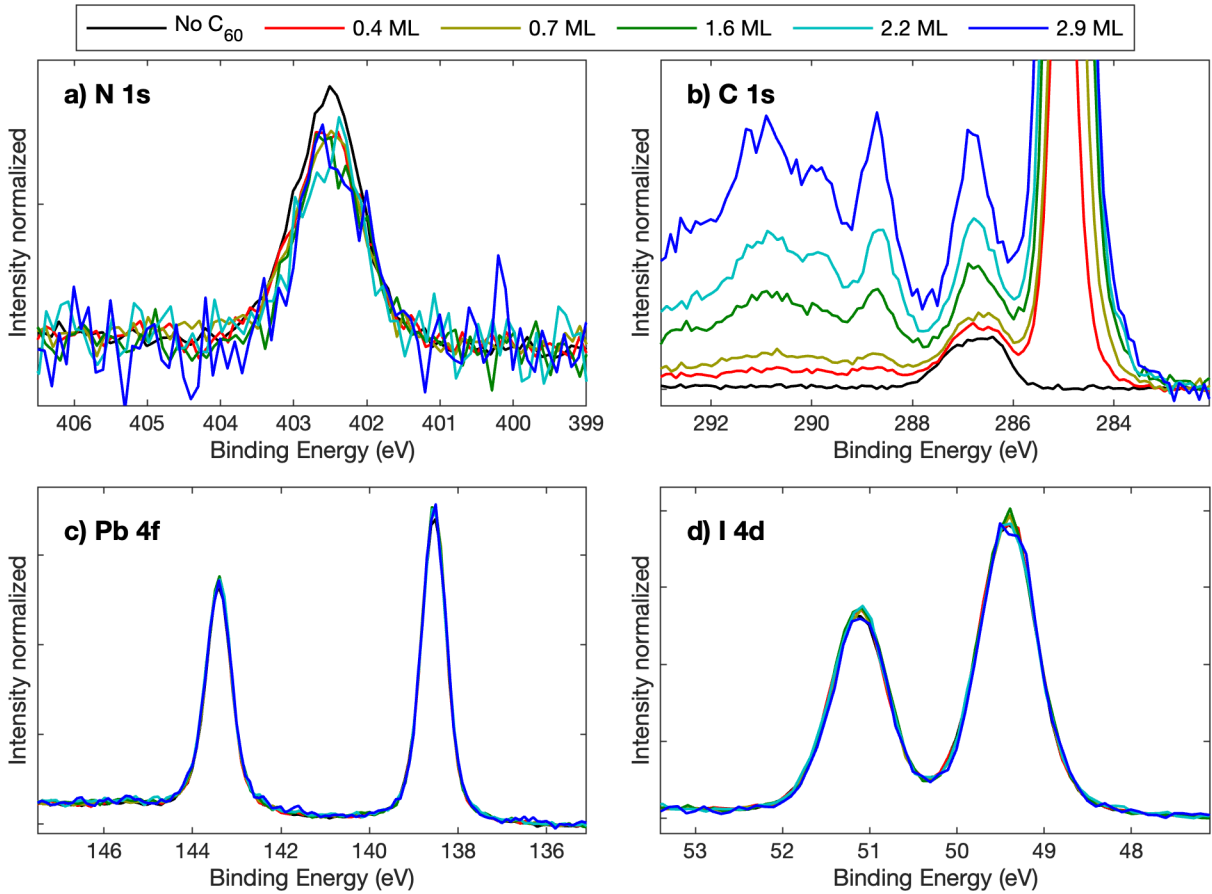


Fig 3. Normalized core level spectra of a) N1s, b) C 1s, c) Pb 4f, d) I 4d of a  $\text{MAPbI}_3$  single crystal surface in Exp 1, spot 1 after cleaving and after consecutive evaporation of  $\text{C}_{60}$  recorded with a photon energy of 535 eV. The binding energy scale is calibrated by setting the  $\text{Pb } 4f_{7/2}$  position to 138.54 eV<sup>29</sup> and the intensities are normalized to the  $\text{Pb } 4f$  intensity. The y-axis of the C 1s spectra is zoomed in to focus on the perovskite peaks and  $\text{C}_{60}$  satellite peaks.

clearly shows that the satellite features are observed at the expected binding energies for all evaporation with the same relative intensities. This confirms that the  $\text{C}_{60}$  molecule is intact upon evaporation and that its electronic structure is not significantly changed. Further evidence for this is found in valence band spectra, where the contribution of the perovskite has been subtracted (Fig S16), which clearly show the same peaks after the different evaporation.

The shape of the C 1s  $\text{C}_{60}$  spectra can be compared to spectra obtained after evaporation of  $\text{C}_{60}$  onto a sputtered gold foil (Fig 4b). On gold, the  $\text{C}_{60}$  spectra are considerably broadened and shifted to much lower binding energies at sub-monolayer coverages.<sup>36,37</sup> Furthermore, the satellites peaks have a different shape at low coverage. From the second layer onwards, the spectral shape resembles that of bulk  $\text{C}_{60}$ . The broadening of the first monolayer is due to the chemisorption of the first monolayer on the metal substrate, where the metal's electron density screens the C 1s core hole leading to a different final state energy and therefore a lower binding energy. Such effects have been observed for  $\text{C}_{60}$  on different metals but should not be observed when  $\text{C}_{60}$  is adsorbed on a semiconductor.<sup>36-40</sup> The initial broadening of the  $\text{C}_{60}$  main peak on  $\text{MAPbI}_3$  could be interpreted in two ways: interaction between the perovskite and  $\text{C}_{60}$  or a broadening at coverages

less than one monolayer. Overall, this indicates that there is a different interaction between  $\text{C}_{60}$  and  $\text{MAPbI}_3$  than in between  $\text{C}_{60}$  molecules, however the effect of this interaction on the electronic structure of  $\text{C}_{60}$  is small.

Given that both perovskite and  $\text{C}_{60}$  remain intact during evaporation and that there are only minor changes in the electronic structure, the shifts in core level positions can be used to determine the energy alignment at the  $\text{MAPbI}_3$  /  $\text{C}_{60}$  interface based on a rigid band model.<sup>41</sup> In this model, the energy difference between core levels and valence and conduction band is assumed to be constant for a given material and core level positions can thus be used to follow changes in the band alignment. For the perovskite, this effect can also be observed in overlapping core level positions for the N 1s and I 4d core levels after evaporation when calibrated to the  $\text{Pb } 4f_{7/2}$  position (Fig 3). In the following, we will focus on using the  $\text{Pb } 4f_{7/2}$  position of the perovskite and the C 1s position of the main  $\text{C}_{60}$  peak to follow the band alignment at the perovskite /  $\text{C}_{60}$  interface.

Fig 5a and b show the positions of the  $\text{Pb } 4f_{7/2}$  peak of the perovskite and the C 1s peak of the  $\text{C}_{60}$  calibrated to the Fermi level as described above during the consecutive evaporation determined from measurements in two different spots on the

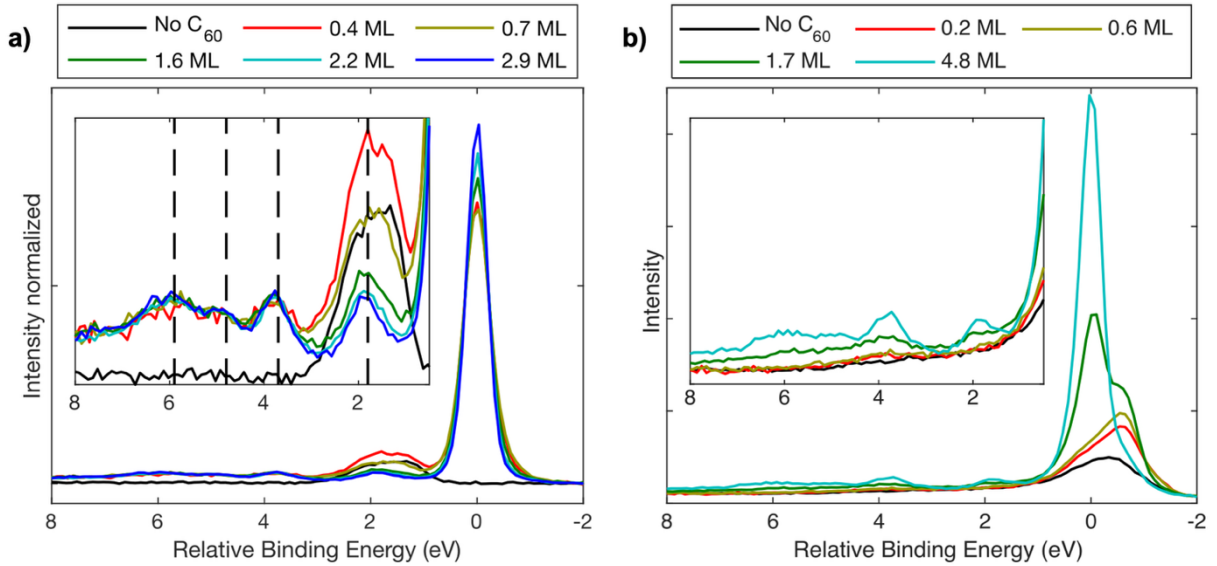


**Fig 4.** a) C 1s spectra of a MAPbI<sub>3</sub> single crystal surface after cleaving in Exp 1, spot 1 and after consecutive evaporation of C<sub>60</sub> recorded with a photon energy of 535 eV relative to the position of the main C<sub>60</sub> C 1s peak and normalized to its intensity. In the inset, a zoom on the region containing the C<sub>60</sub> satellite peaks is shown with the expected positions indicated by dashed vertical lines. b) C 1s spectra of C<sub>60</sub> evaporated onto a gold foil in Exp 2 recorded with a photon energy of 535 eV relative to the position of the main C<sub>60</sub> peak in the 4.8 ML measurement. In the inset, a zoom on the region containing the C<sub>60</sub> satellite peaks is shown.

sample and at two different photon energies (535 eV, 758 eV) in Exp 1. It can be seen that the Pb 4f<sub>7/2</sub> position is quite constant (shifts of less than 0.05 eV for different evaporation within one measurement set). However, some variations for the different spots and photon energies are observed with peak positions shifting to higher binding energies upon addition of more C<sub>60</sub> in spot 1 and to lower binding energies in spot 2. For the C 1s core level of C<sub>60</sub>, a shift to lower binding energy is observed with increasing amount of C<sub>60</sub>. However, the absolute positions vary between different spots, and the observed shift is more gradual in spot 2. Overall, the differences in trends and absolute binding energy position highlight the need for repeated experiments. Differences in absolute binding energies can stem from differences in Fermi level position but also from sample charging effects under X-ray illumination.

To get further insight, we used a data analysis method for comparing the three different C<sub>60</sub> evaporation experiments on MAPbI<sub>3</sub>, (Exp 1, 2 and 3), which is based on the energy difference between the C<sub>60</sub> C 1s peak and the perovskite Pb 4f<sub>7/2</sub> peak (described in the next section). In one of the experiments (Exp 3), we observed some sample charging with the Pb 4f<sub>7/2</sub> core level position being at higher binding energy than in previous experiments (Fig S12-S14). To estimate the effect of sample charging on our analysis, the substrate and overlayer system was measured at different incident X-ray flux values (Fig S15). While the measured absolute binding energy of the Pb 4f and C 1s core level increases as a function of incident photon flux, the energetic difference between the core levels remains constant (Fig S17). Hence, we conclude that charging events do not impact the presented analysis. In contrast, such effects will impact an analysis based on absolute energy positions, such as valence band edge determinations and secondary electron cutoff measurements to determine the work function.

### Energy alignment

To be able to compare different C<sub>60</sub> evaporation experiments, we focused on determining an energy offset parameter between C<sub>60</sub> and MAPbI<sub>3</sub> for the different evaporation. In this way, the energy offset can be plotted versus the C<sub>60</sub> thickness in monolayers (determined from the Pb 4f core level intensity as described in the experimental and in the SI).

To calculate the energy offset, the binding energy positions of the Pb 4f<sub>7/2</sub> (perovskite) and the C 1s (C<sub>60</sub>) recorded after evaporation were used. Additionally, the energy difference between the Pb 4f<sub>7/2</sub> and the valence band edge was determined from a combination of core level and valence band measurements, which were energy calibrated internally (Fig S18 and S19). A value of 137.39 eV was found for the Pb 4f<sub>7/2</sub> core level position, which is very similar to values found previously for mixed cation lead iodide perovskites thin films but somewhat higher than a value determined for MAPbI<sub>3</sub> thin films.<sup>42,43</sup> For C<sub>60</sub>, an energy difference between C 1s and the HOMO level (defined here as the onset energy of the HOMO peak) was determined to be 283.24 eV (Fig S20 and S21).<sup>44,45</sup> From these values, the energy offset between the perovskite valence band (VB) and the C<sub>60</sub> HOMO level can be determined from the Pb 4f<sub>7/2</sub> and C 1s position according to the following equation:

$$\Delta E_{HOMO-VB} = (E_{C\ 1s} - 283.24\ eV) - (E_{Pb\ 4f_{7/2}} - 137.39\ eV).$$

Fig 6a shows a schematic energy diagram, where these differences are indicated. Note that a positive  $\Delta E_{HOMO-VB}$  signifies that the C<sub>60</sub> HOMO level is below the perovskite valence band in energy (as indicated in Fig 6a). Fig 6b shows the values of  $\Delta E_{HOMO-VB}$  at different monolayer thicknesses  $d_{ML}$  for

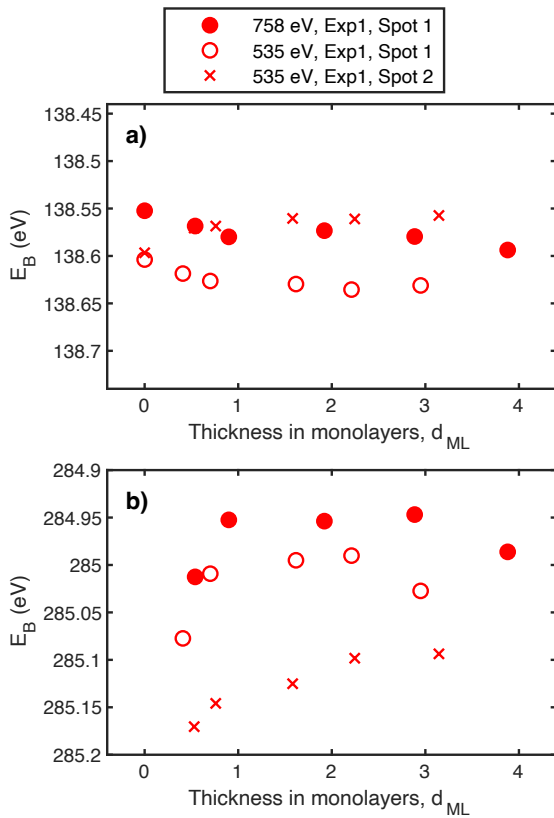


**Fig 5.** Peak position calibrated to the Fermi level of a)  $\text{Pb } 4f_{1/2}$  (perovskite peak) and b)  $\text{C } 1s$  ( $\text{C}_{60}$  peak) after different evaporation of  $\text{C}_{60}$ , determined from Exp 1 in 2 different spots on the sample and at two different photon energies (535 eV and 758 eV).

all three experiments in all measurement spots. All calculated values are positive and therefore indicate hole blocking properties of  $\text{C}_{60}$  at the interface to the perovskite, which is desirable for the function of solar cells. Measurements in the same spot with 535 and 758 eV photon energy give similar energy offset values but appear at slightly different points on the x-axis which can be explained by the uncertainty in the

determined thicknesses (Fig S4). However, the data exhibits an energetic spread at low coverages below 3 ML of up to 0.2 eV between different spots and across Exp 1 and 2 showing that the energy offset at low coverages is not always the same. Quarti et al. suggested that the surface termination can impact the energetic alignment of  $\text{C}_{60}$  on  $\text{MAPbI}_3$  as demonstrated through calculations.<sup>28</sup> A similar dependence on the surface termination has also been previously reported for the  $\text{CsPbBr}_3/\text{C}_{60}$  interface.<sup>22</sup> Loh et al. determine a 0.4 eV shift of the molecular orbitals between  $\text{CsBr}$  and  $\text{PbBr}_2$  termination. In the present case, the core level spectra of the cleaved  $\text{MAPbI}_3$  surfaces at both 535 eV and 758 eV show very similar relative core level intensities. We therefore do not see any evidence for significant differences in the surface termination between spots and samples, as these should change the relative core level intensities.<sup>46</sup> However, we note that spot 1 in Exp 1 was cleaner than the other measurement spots without the presence of any adventitious carbon (Fig 1 and Fig S5-6). This spot shows a lower value of the energy offset at low coverages compared to all other measurement spots. This suggests that in addition to surface termination, also the presence of surface contaminants can influence the energy alignment between  $\text{MAPbI}_3$  and  $\text{C}_{60}$ . Despite the observed spread in the initial alignment, the values for  $\Delta E_{HOMO-VB}$  become smaller at higher values of  $d_{ML}$  in all measurement spots in all experiments. This general trend indicates a downward energy shift in the  $\text{C}_{60}$  layer towards the interface with  $\text{MAPbI}_3$ , which can be interpreted as downwards band bending in agreement with some previous reports.<sup>25,26</sup> Furthermore, at higher coverages the values tend to an energy offset of 0.52 eV between the  $\text{MAPbI}_3$  valence band and the  $\text{C}_{60}$  HOMO level. This value is significantly larger compared to 0.10 eV reported by Lo et al.<sup>25</sup> while good agreement is present with Wang et al. who report 0.57 eV.<sup>26</sup>

Based on our observations, we construct an energy diagram for the  $\text{MAPbI}_3/\text{C}_{60}$  interface (Fig 7). In this diagram, we also include

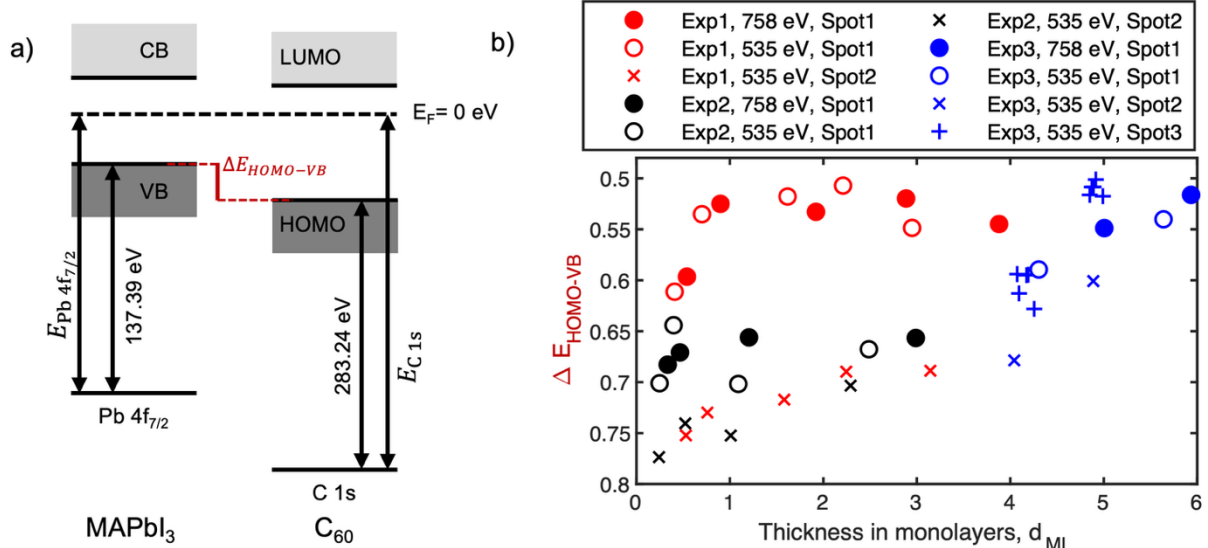


**Fig 6.** a) Energy diagram indicating how  $\Delta E_{HOMO-VB}$  is defined and calculated. b) Calculated  $\Delta E_{HOMO-VB}$  plotted vs.  $\text{C}_{60}$  thickness in monolayers,  $d_{ML}$ , determined from  $\text{Pb } 4f_{7/2}$  and  $\text{C } 1s$  core level measurements after  $\text{C}_{60}$  evaporation on  $\text{MAPbI}_3$  single crystal surfaces. The different colors indicate three different evaporation series on three different  $\text{MAPbI}_3$  single crystals. The different symbols indicate different photon energies (535 eV and 758 eV) and measurement spots on the sample.

the conduction band edge of  $\text{MAPbI}_3$  at 1.57 eV above the valence band edge based on the bandgap ( $E_g$ ) of  $\text{MAPbI}_3$ .<sup>47</sup> Additionally, the LUMO of  $\text{C}_{60}$  is calculated in the same way. However, for  $\text{C}_{60}$ , different HOMO-LUMO gaps have been reported and applied. Typical values are often between 1.7 and 1.92 eV.<sup>21,48,49</sup> Yet, in some band diagrams with perovskites a larger value of 2.3 eV was used, which had been determined by a combination of UPS and IPES measurements.<sup>24,25</sup> In our band diagram we therefore indicate two  $\text{C}_{60}$  LUMO positions, one based on a bandgap of 1.86 eV,<sup>48</sup> which is also the value we use in the mean free path calculations, and one based on 2.3 eV. In the case of a band gap of 1.86 eV, the LUMO of  $\text{C}_{60}$  is always below the conduction band edge of  $\text{MAPbI}_3$  as needed for successful charge extraction, with an energy offset between the LUMO and the conduction band of 0.25 eV at higher  $\text{C}_{60}$  thicknesses. In case of a bandgap of 2.3 eV, the LUMO of  $\text{C}_{60}$  is above the conduction band of perovskite, which would be unfavorable for charge extraction. As  $\text{C}_{60}$  is used successfully as an electron selective contact in perovskite solar cells, these discrepancies can be interpreted in the following ways: 1. A lower band gap is the more correct value to use, as the combination of UPS and IPES might overestimate the band gap or 2. the additional layers in a device, such as charge blocking layers and metal contacts lead to a further modification of the energetic landscape, which enables efficient charge extraction. The latter is also a focus of further studies by our group.

Overall, our results indicate that the energy alignment between  $\text{MAPbI}_3$  and  $\text{C}_{60}$  may vary and is very sensitive to the exact surface composition, which includes the exact termination and/or very small amounts of surface contamination. This result explains the spread of values found in literature to some degree. In particular, when using multicrystalline thin films of  $\text{MAPbI}_3$ , the surface chemistry of the  $\text{MAPbI}_3$  can vary significantly with the exact preparation procedure and environment. Furthermore,  $\text{C}_{60}$  shows some downward energy shifts towards the perovskite, which is unfavorable for charge extraction and could lead to charge trapping at the interface. This can explain the need for passivation molecules and additional charge blocking layers in efficient solar cells. Our results show that, without the use of further surface treatment, the energy offset between  $\text{MAPbI}_3$  and the perovskite reaches a constant value at thicknesses of about 5 ML.

## Conclusions

In conclusion, we investigated the energy alignment of  $\text{C}_{60}$  on cleaved  $\text{MAPbI}_3$  single crystal surfaces in several in-situ experiments. We find that both  $\text{MAPbI}_3$  and  $\text{C}_{60}$  remain intact upon interface formation unlike what is observed for evaporation of metals on perovskite surfaces. Furthermore, our results indicate some interaction between thin layers of  $\text{C}_{60}$  and the perovskite, but no significant changes to the electronic structure.

By determining the thickness of the evaporated  $\text{C}_{60}$  layer from the Pb 4f core level intensity attenuation and the energy offset

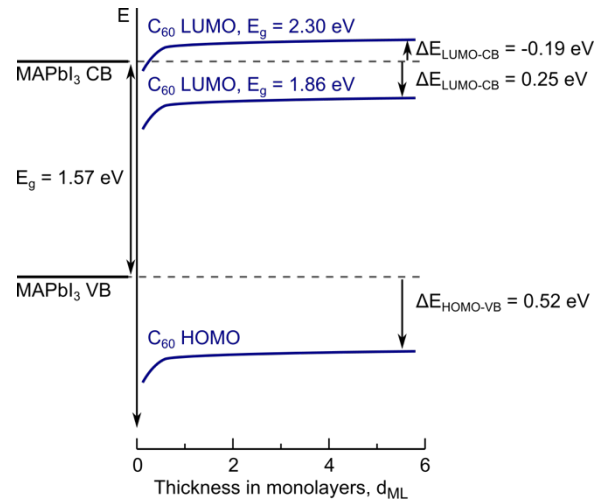


Fig 7. Energy diagram of the  $\text{MAPbI}_3/\text{C}_{60}$  interface constructed based on the data in Fig 6b and band gap values for  $\text{MAPbI}_3$  and for  $\text{C}_{60}$  as discussed.

between the  $\text{MAPbI}_3$  valence band and the  $\text{C}_{60}$  HOMO level from relative core level positions, we are able to compare a series of different repeat experiments. We find that  $\text{C}_{60}$  shows a downward energy shift toward  $\text{MAPbI}_3$  in repeat experiments, similar to what others have reported previously. However, the magnitude of the energy shift varied between different experiments, potentially due to differences in surface termination or the presence of adventitious carbon on the surface. When the coverage of  $\text{C}_{60}$  reached several monolayers, the energy offset between the HOMO and the valence band became constant at 0.52 eV. When assuming a  $\text{C}_{60}$  HOMO-LUMO gap of 1.86 eV, the LUMO of  $\text{C}_{60}$  is 0.25 eV below the conduction band of  $\text{MAPbI}_3$ , which is favorable for charge extraction. A HOMO-LUMO gap of 2.3 eV, which has been used in some studies, would suggest that the  $\text{C}_{60}$  LUMO is above the  $\text{MAPbI}_3$  conduction band by 0.19 eV, i.e. too high for charge extraction. This value as well as the unfavorable energy shift could explain why further interface modification, for example by charge blocking layers, is needed for efficient solar cells when using  $\text{C}_{60}$  as an ETL. Overall, our study highlights that energy alignment directly at the interface in perovskite solar cells can vary between different repeat experiments, even for single crystals, and it therefore is very sensitive to the exact surface composition. This means great care has to be taken in determining the energy alignment for a given system.

## Author contributions

A.G.-F.: Conceptualization, Formal analysis, Investigation, Writing – original draft, Visualization, Resources K.R.: Conceptualization, Formal analysis, Investigation, Writing – original draft, review and editing, Visualization S.R.: Investigation, Writing – review and editing, B.K.: Investigation, Writing – review and editing, E.J.: Investigation, Writing – review and editing, R.M.: Investigation, Writing – review and editing, H.R.: Project administration, Funding acquisition, Writing – review and editing, U.B.C.: Conceptualization, Formal analysis, Investigation, Writing – original draft, review and editing,

Visualization, Project administration, Funding acquisition, Supervision.

## Conflicts of interest

There are no conflicts to declare.

## Data availability

The data supporting this article have been included within the article and as part of the Supplementary Information. Supplementary information: Details on thickness calculation, additional photoelectron spectroscopy data and analysis. See DOI: [URL – format <https://doi.org/DOI>]

## Acknowledgements

We acknowledge the MAX IV Laboratory for beamtime on the FlexPES beamline under proposal 20220600, 20230156, and 20240429. Research conducted at MAX IV, a Swedish national user facility, is supported by Vetenskapsrådet (Swedish Research Council, VR) under contract 2018-07152, Vinnova (Swedish Governmental Agency for Innovation Systems) under contract 2018-04969 and Formas under contract 2019-02496. We thank Alexei Preobrajenski, Stephan Appelfeller, and Alexander Generalov for their support during the beamtime. This work was partially supported by the Wallenberg Initiative Materials Science for Sustainability (WISE) funded by the Knut and Alice Wallenberg Foundation. We thank the Swedish Research Council (Grant numbers 2022-03168 and 2023-05072) for funding. A.G.-F acknowledges support from a Beatriz Galindo junior fellowship (BG23/00033) from the Spanish Ministry of Science and Innovation. S.R. and H.R. acknowledge support from the Swedish Energy Agency (P50626-1).

## Notes and references

- 1 J. J. Yoo, S. S. Shin and J. Seo, *ACS Energy Lett.*, 2022, 7, 2084–2091.
- 2 M. A. Green, A. Ho-Baillie and H. J. Snaith, *Nat Photonics*, 2014, 8, 506–514.
- 3 P. Wang, Y. Wu, B. Cai, Q. Ma, X. Zheng and W.-H. Zhang, *Adv Funct Mater.*, 2019, 29, 1807661.
- 4 B. Roose, Q. Wang and A. Abate, *Adv Energy Mater.*, 2019, 9, 1803140.
- 5 L. Deng, S. Xie and F. Gao, *Adv Electron Mater.*, 2018, 4, 1700435.
- 6 Y. Zheng, J. Kong, D. Huang, W. Shi, L. McMillon-Brown, H. E. Katz, J. Yu and A. D. Taylor, *Nanoscale*, 2018, 10, 11342–11348.
- 7 C.-H. Chiang and C.-G. Wu, *Nat Photonics*, 2016, 10, 196–200.
- 8 C. Gong, H. Li, Z. Xu, Y. Li, H. Wang, Q. Zhuang, A. Wang, Z. Li, Z. Guo, C. Zhang, B. Wang, X. Li and Z. Zang, *Nat Commun.*, 2024, 15, 9154.
- 9 M. M. Elnaggar and N. A. Emelianov, *Applied Physics A*, 2024, 130, 471.
- 10 H.-J. Lee and S.-I. Na, *J Alloys Compd.*, 2022, 921, 166007.
- 11 D. Yu, M. Pan, G. Liu, X. Jiang, X. Wen, W. Li, S. Chen, W. Zhou, H. Wang, Y. Lu, M. Ma, Z. Zang, P. Cheng, Q. Ji, F. Zheng and Z. Ning, *Nat Energy*, 2024, 9, 298–307.
- 12 C. Momblona, L. Gil-Escríg, E. Bandiello, E. M. Hutter, M. Sessolo, K. Lederer, J. Blochwitz-Nimoth and H. J. Bolink, *Energy Environ Sci.*, 2016, 9, 3456–3463.
- 13 J. Suo, B. Yang, E. Mosconi, D. Bogachuk, T. A. S. Doherty, K. Frohna, D. J. Kubicki, F. Fu, Y. Kim and O. Er-Raji, *Nat Energy*, 2024, 9, 172–183.
- 14 T. Nguyen, D. Yeo, R. K. Chitumalla, S. Kim, G. Jeong, D. Kwun, J. Jang, I. H. Jung and J. Seo, *Adv Energy Mater.*, 2025, 15, 2403633.
- 15 S.-G. Choi, S.-K. Jung, J.-H. Lee, J.-H. Kim, W. Zheng and J.-W. Lee, *ACS Energy Lett.*, 2024, 9, 5360–5363.
- 16 W. Li, G. Wang, Y. Long, L. Xiao, Z. Zhong, X. Li, H. Xu, H. Yan and Q. Song, *ACS Appl Mater Interfaces*, 2024, 16, 63019–63025.
- 17 A. A. Said, E. Aydin, E. Ugur, Z. Xu, C. Deger, B. Vishal, A. Vlk, P. Dally, B. K. Yildirim, R. Azmi, J. Liu, E. A. Jackson, H. M. Johnson, M. Gui, H. Richter, A. R. Pininti, H. Bristow, M. Babics, A. Razzaq, S. Mandal, T. G. Allen, T. D. Anthopoulos, M. Ledinský, I. Yavuz, B. P. Rand and S. De Wolf, *Nat Commun.*, 2024, 15, 708.
- 18 J. Zhang, Z. He and C. Chen, *J Mater Chem A Mater.*, 2025.
- 19 S. Hu, J. Wang, P. Zhao, J. Pascual, J. Wang, F. Rombach, A. Dasgupta, W. Liu, M. A. Truong, H. Zhu, M. Kober-Czerny, J. N. Drysdale, J. A. Smith, Z. Yuan, G. J. W. Aalbers, N. R. M. Schipper, J. Yao, K. Nakano, S.-H. Turren-Cruz, A. Dallmann, M. G. Christoforo, J. M. Ball, D. P. McMeekin, K.-A. Zaininger, Z. Liu, N. K. Noel, K. Tajima, W. Chen, M. Ehara, R. A. J. Janssen, A. Wakamiya and H. J. Snaith, *Nature*, 2025, 639, 93–101.
- 20 S. Wang, T. Sakurai, W. Wen and Y. Qi, *Adv Mater Interfaces*, 2018, 5, 1800260.

- 21 D. Menzel, A. Al-Ashouri, A. Tejada, I. Levine, J. A. Guerra, B. Rech, S. Albrecht and L. Korte, *Adv Energy Mater*, 2022, 12, 2201109.
- 22 H. Loh, A. Raabgrund and M. A. Schneider, *ACS Nano*, 2025, 19, 10199–10206.
- 23 J.-Y. Jeng, Y.-F. Chiang, M.-H. Lee, S.-R. Peng, T.-F. Guo, P. Chen and T.-C. Wen, *Advanced Materials*, 2013, 25, 3727–3732.
- 24 P. Schulz, L. L. Whittaker-Brooks, B. A. MacLeod, D. C. Olson, Y.-L. Loo and A. Kahn, *Adv Mater Interfaces*, 2015, 2, 1400532.
- 25 M.-F. Lo, Z.-Q. Guan, T.-W. Ng, C.-Y. Chan and C.-S. Lee, *Adv Funct Mater*, 2015, 25, 1213–1218.
- 26 C. Wang, C. Wang, X. Liu, J. Kauppi, Y. Shao, Z. Xiao, C. Bi, J. Huang and Y. Gao, *Appl Phys Lett*, 2015, 106, 111603.
- 27 D. Shin, D. Kang, J. Jeong, S. Park, M. Kim, H. Lee and Y. Yi, *Phys Chem Lett*, 2017, 8, 5423–5429.
- 28 C. Quarti, F. De Angelis and D. Beljonne, *Chemistry of Materials*, 2017, 29, 958–968.
- 29 A. García-Fernández, S. Svanström, C. M. Sterling, A. Gangan, A. Erbing, C. Kamal, T. Sloboda, B. Kammlander, G. J. Man, H. Rensmo, M. Odelius and U. B. Cappel, *Small*, 2022, 18, 2106450.
- 30 A. Preobrajenski, A. Generalov, G. Öhrwall, M. Tchaplyguine, H. Tarawneh, S. Appelfeller, E. Frampton and N. Walsh, *Synchrotron Radiation*, 2023, 30, 831–840.
- 31 S. Liu, Y.-J. Lu, M. M. Kappes and J. A. Ibers, *Science (1979)*, 1991, 254, 408–410.
- 32 S. Tanuma, C. J. Powell and D. R. Penn, *Surface and interface analysis*, 2003, 35, 268–275.
- 33 S. Svanstrom, T. J. Jacobsson, G. Boschloo, E. M. J. Johansson, H. Rensmo and U. B. Cappel, *ACS Appl Mater Interfaces*, 2020, 12, 7212–7221.
- 34 S. Svanström, A. García-Fernández, T. J. Jacobsson, I. Bidermane, T. Leitner, T. Sloboda, G. J. Man, G. Boschloo, E. M. J. Johansson and H. Rensmo, *ACS materials Au*, 2022, 2, 301–312.
- 35 C. Enkvist, S. Lunell, B. Sjögren, S. Svensson, P. A. Brühwiler, A. Nilsson, A. J. Maxwell and N. Mårtensson, *Phys Rev B*, 1993, 48, 14629.
- 36 A. J. Maxwell, P. A. Brühwiler, A. Nilsson, N. Mårtensson and P. Rudolf, *Phys Rev B*, 1994, 49, 10717.
- 37 A. J. Maxwell, P. A. Brühwiler, D. Arvanitis, J. Hasselström and N. Mårtensson, *Chem Phys Lett*, 1996, 260, 71–77.
- 38 E. Magnano, S. Vandré, C. Cepek, A. Goldoni, A. D. Laine, G. M. Curró, A. Santaniello and M. Sancrotti, *Surf Sci*, 1997, 377–379, 1066–1070.
- 39 K. Sakamoto, D. Kondo, M. Harada, A. Kimura, A. Kakizaki and S. Suto, *Surf Sci*, 1999, 433–435, 642–646.
- 40 T. R. Ohno, Y. Chen, S. E. Harvey, G. H. Kroll, J. H. Weaver, R. E. Haufler and R. E. Smalley, *Phys Rev B*, 1991, 44, 13747.
- 41 E. A. Kraut, R. W. Grant, J. R. Waldrop and S. P. Kowalczyk, *Phys Rev Lett*, 1980, 44, 1620–1623.
- 42 S. Svanström, A. García Fernández, T. Sloboda, T. J. Jacobsson, F. Zhang, F. O. L. Johansson, D. Kühn, D. Céolin, J.-P. Rueff, L. Sun, K. Aitola, H. Rensmo and U. B. Cappel, *ACS Appl Mater Interfaces*, 2023, 15, 12485–12494.
- 43 M. Wussler, T. Mayer, C. Das, E. Mankel, T. Hellmann, C. Prabowo, I. Zimmermann, M. K. Nazeeruddin and W. Jaegermann, *Adv Funct Mater*, 2020, 30, 1910679.
- 44 M. Shibuta, K. Yamamoto, T. Ohta, M. Nakaya, T. Eguchi and A. Nakajima, *Sci Rep*, 2016, 6, 35853.
- 45 J. H. Seo, S. J. Kang, C. Y. Kim, S. W. Cho, K.-H. Yoo and C. N. Whang, *Appl Surf Sci*, 2006, 252, 8015–8017.
- 46 G. J. Man, C. M. Sterling, C. Kamal, K. A. Simonov, S. Svanström, J. Acharya, F. O. L. Johansson, E. Giangrisostomi, R. Ovsyannikov and T. Huthwelker, *Phys Rev B*, 2021, 104, L041302.
- 47 S. A. Kulkarni, T. Baikie, P. P. Boix, N. Yantara, N. Mathews and S. Mhaisalkar, *J Mater Chem A Mater*, 2014, 2, 9221–9225.
- 48 T. Rabenau, A. Simon, R. K. Kremer and E. Sohmen, *Zeitschrift für Physik B Condensed Matter*, 1993, 90, 69–72.
- 49 B. Miller, J. M. Rosamilia, G. Dabbagh, R. Tycko, R. C. Haddon, A. J. Muller, W. Wilson, D. W. Murphy and A. F. Hebard, *J Am Chem Soc*, 1991, 113, 6291–6293.

## Supplementary Information for:

# Resolving the energy alignment between methylammonium lead iodide and C<sub>60</sub>: an in-situ photoelectron spectroscopy study

Alberto García-Fernández, Karen Radetzky, Stefania Riva, Birgit Kammlander, Brian Rydgren, Evelyn Johannesson, Rahul Mahavir Varma, Håkan Rensmo, Ute B. Cappel

Table S1. Parameters used in the inelastic mean free path calculations.<sup>1,2</sup>

| Core level | Photon energy [eV] | E <sub>kin</sub> [eV] | C <sub>60</sub> density [g/cm <sup>3</sup> ] | C <sub>60</sub> molar mass [g/mol] | C <sub>60</sub> valence electrons | C <sub>60</sub> band gap | IMFP [nm] |
|------------|--------------------|-----------------------|--|------------------------------------|-----------------------------------|--------------------------|-----------|
| Pb 4f      | 535                | 396                   | 1.65   | 720.66                             | 240                               | 1.86                     | 1.35      |
| Pb 4f      | 758                | 619                   | 1.65   | 720.66                             | 240                               | 1.86                     | 1.87      |
| Au 4f      | 535                | 451                   | 1.65   | 720.66                             | 240                               | 1.86                     | 1.48      |

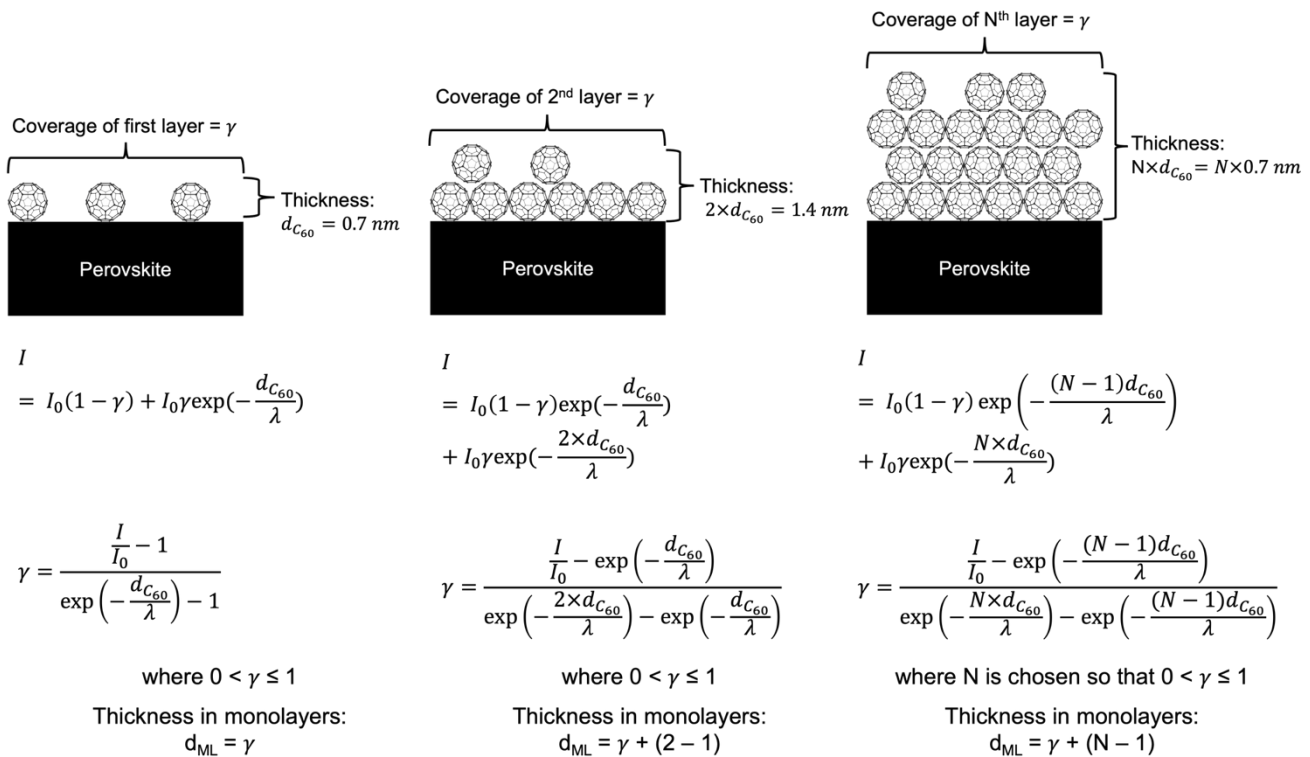


Figure S1: Model 1 for calculating the thickness in number of monolayers of C<sub>60</sub>. The model is based on the assumption that the C<sub>60</sub> layer on the surface forms layer-by-layer and that the thickness of one monolayer of C<sub>60</sub> ( $d_{C_{60}}$ ) is 0.7 nm (diameter of C<sub>60</sub>).<sup>3</sup>  $I_0$  describes the intensity of a given perovskite core level (Pb 4f was used for the calculations in this paper) without C<sub>60</sub> on top, while  $I$  is the intensity of the same core level measured with the same experimental settings after deposition of C<sub>60</sub>.  $\lambda$  is the inelastic mean free path (IMFP) of the photoelectron.

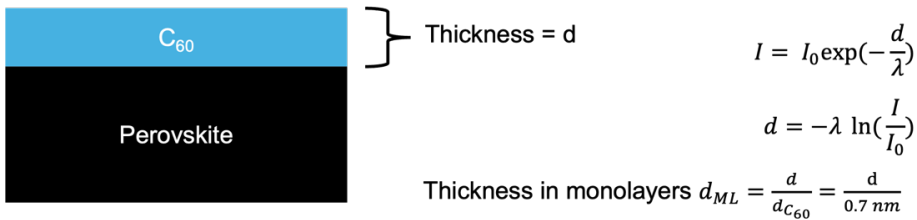


Figure S2: Model 2 for calculating the thickness of  $C_{60}$ . The model is based on the assumption that the  $C_{60}$  layer has a uniform thickness of  $d$ . The thickness in number of monolayers is then obtained by dividing  $d$  by the diameter of  $C_{60}$  (0.7 nm). While this model gives similar values to the one above, a uniform layer thickness is not physically possible for layers below one monolayer.  $I_0$  describes the intensity of a given perovskite core level (Pb 4f was used for the calculations in this paper) without  $C_{60}$  on top, while  $I$  is the intensity of the same core level measured with the same experimental settings after deposition of  $C_{60}$ .  $\lambda$  is the inelastic mean free path (IMFP) of the photoelectron.

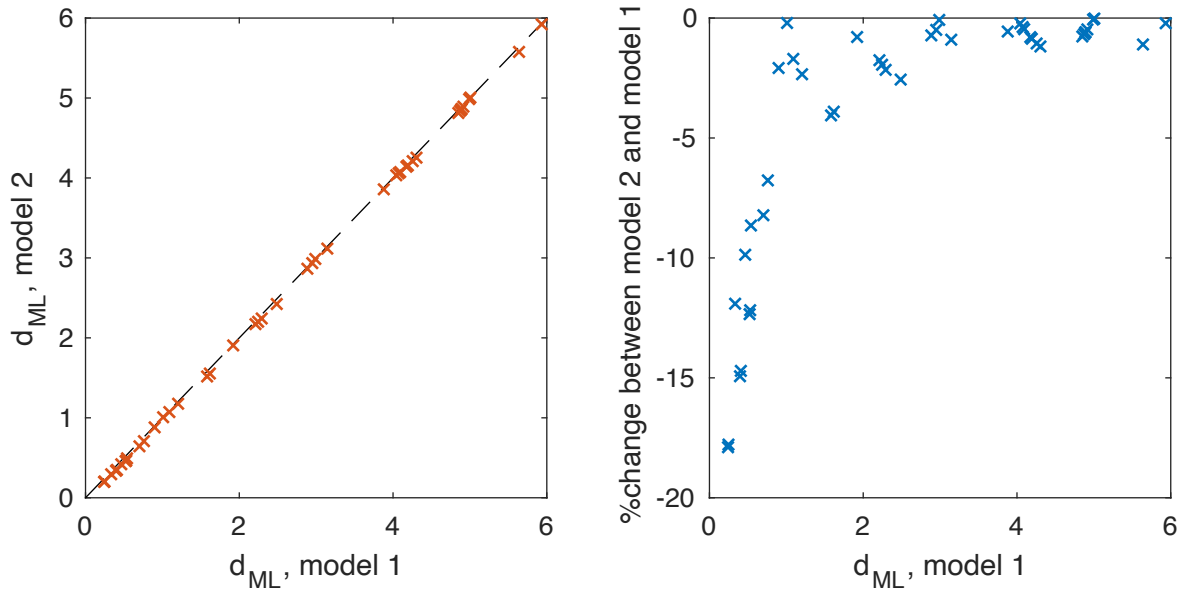


Figure S3: Comparison of the thickness in monolayers ( $d_{ML}$ ) obtained from model 1 and model 2. Left: Values from model 2 plotted versus values from model 1 (red crosses), the black dashed line represents, where values would be equal. Right: Percentage change between model 2 and model 1 calculated as  $(d_{ML}(\text{model2}) - d_{ML}(\text{model1})/d_{ML}(\text{model1}) * 100$ .

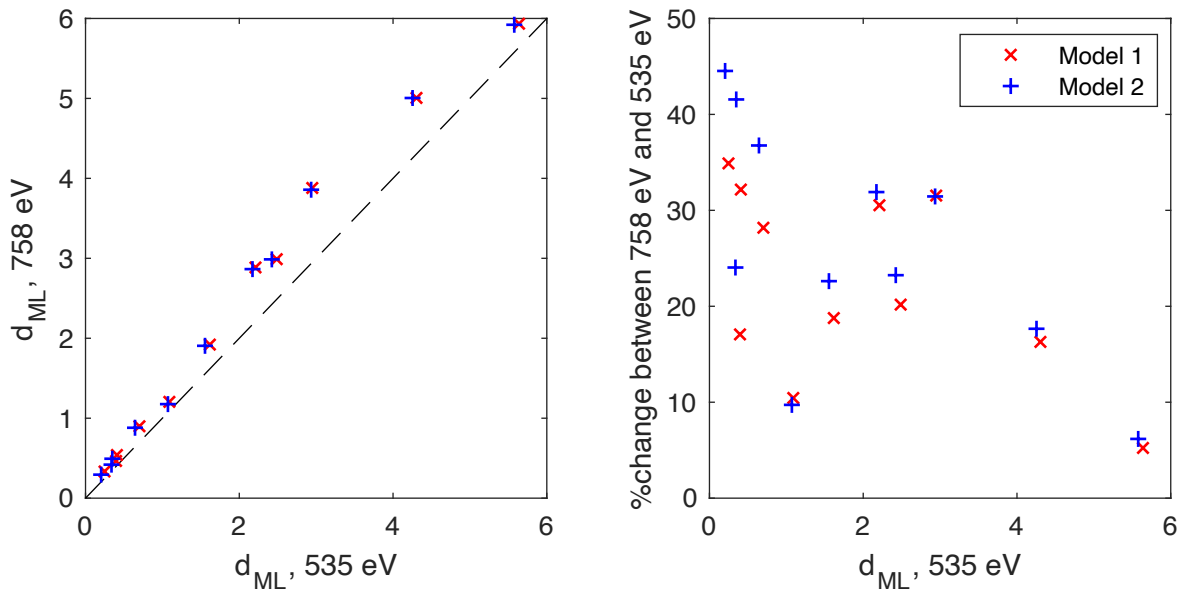


Figure S4: Comparison of the thickness in monolayers ( $d_{ML}$ ) obtained from measurements with two different photon energies (535 eV and 758 eV) on the same spot. Left: Values from 758 eV plotted versus values from 535 eV (red crosses model 1, blue plusses model 2), the black dashed line represents where values would be equal. Right: Percentage change between values at 758 eV and 535 eV calculated as  $((d_{ML}(758 \text{ eV}) - d_{ML}(535 \text{ eV})) / d_{ML}(535 \text{ eV})) * 100$ .

## Discussion of the ML thickness estimation

Model 1 and 2 are in good agreement in particular for higher coverage. At low coverage Model 2 is physically less meaningful and will therefore not give as good an estimate.

The differences in  $d_{ML}$  estimated with the different photon energies can have several origins:

- experimental settings (X-ray intensity, sample position) not always precisely as assumed in the calculations);
- systematic error in the estimation of the mean free path (for example overestimating the relative difference between the mean free path at 535 eV and 758 eV);
- Systematic error in the model used, as it does not account for non-uniform layer formation.

However, it should be noted that the discrepancy between the values (20-30%) is small compared to the thickness range covered in the different experiments (< 1 ML coverage to > 5 ML). Overall, the discrepancy suggests that the error in the thickness estimation is about 30%. Model 1 is used to estimate thicknesses throughout the study.

## Additional photoelectron spectra

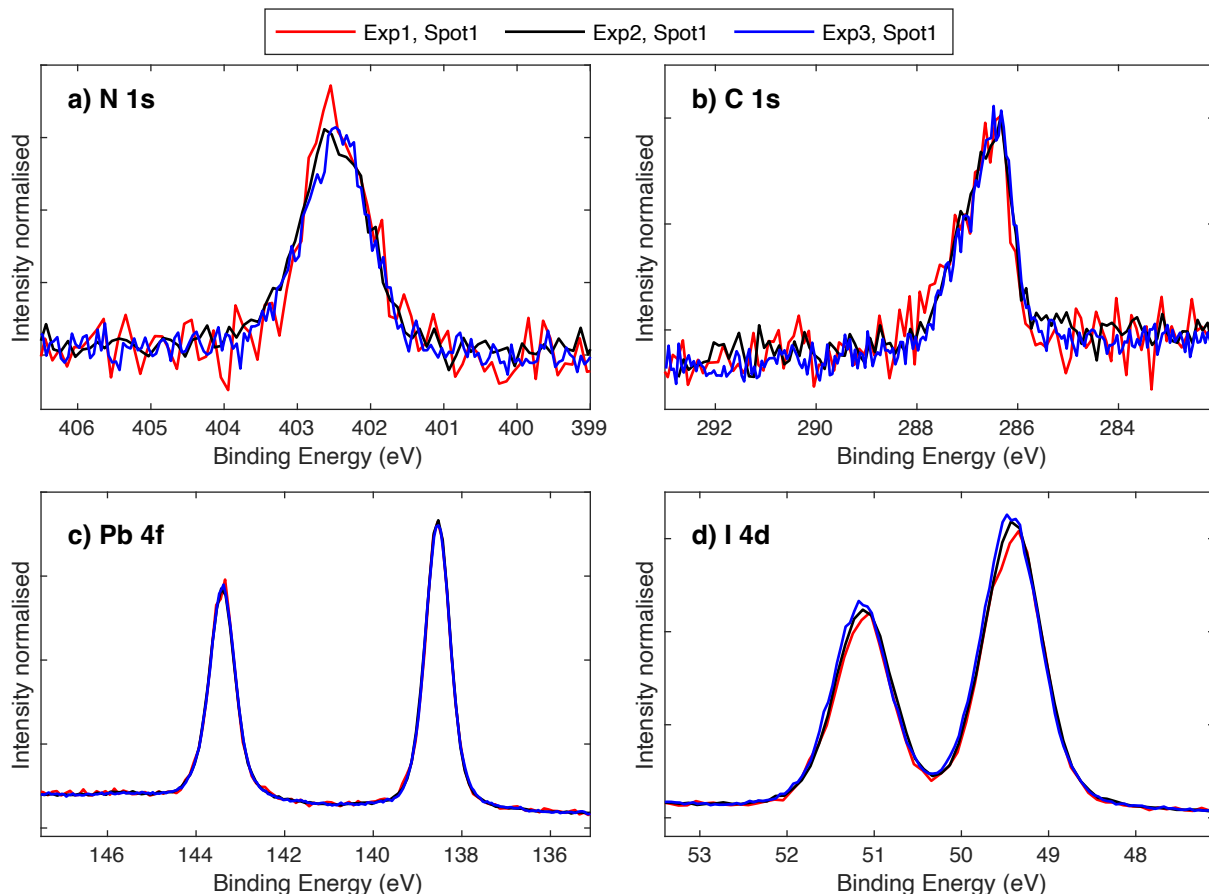


Figure S5: Normalised core level spectra of a) N1s, b) C 1s, c) Pb 4f, d) I 4d of  $\text{MAPbI}_3$  single crystal surfaces after cleaving recorded with a photon energy of 758 eV. Data for three different single crystals measured on three different occasions (Exp1, Exp2 and Exp3) is shown. The binding energy scale is calibrated by setting the  $\text{Pb } 4f_{7/2}$  position to 138.54 eV and the intensities are normalised to the  $\text{Pb } 4f$  intensity.<sup>4</sup>

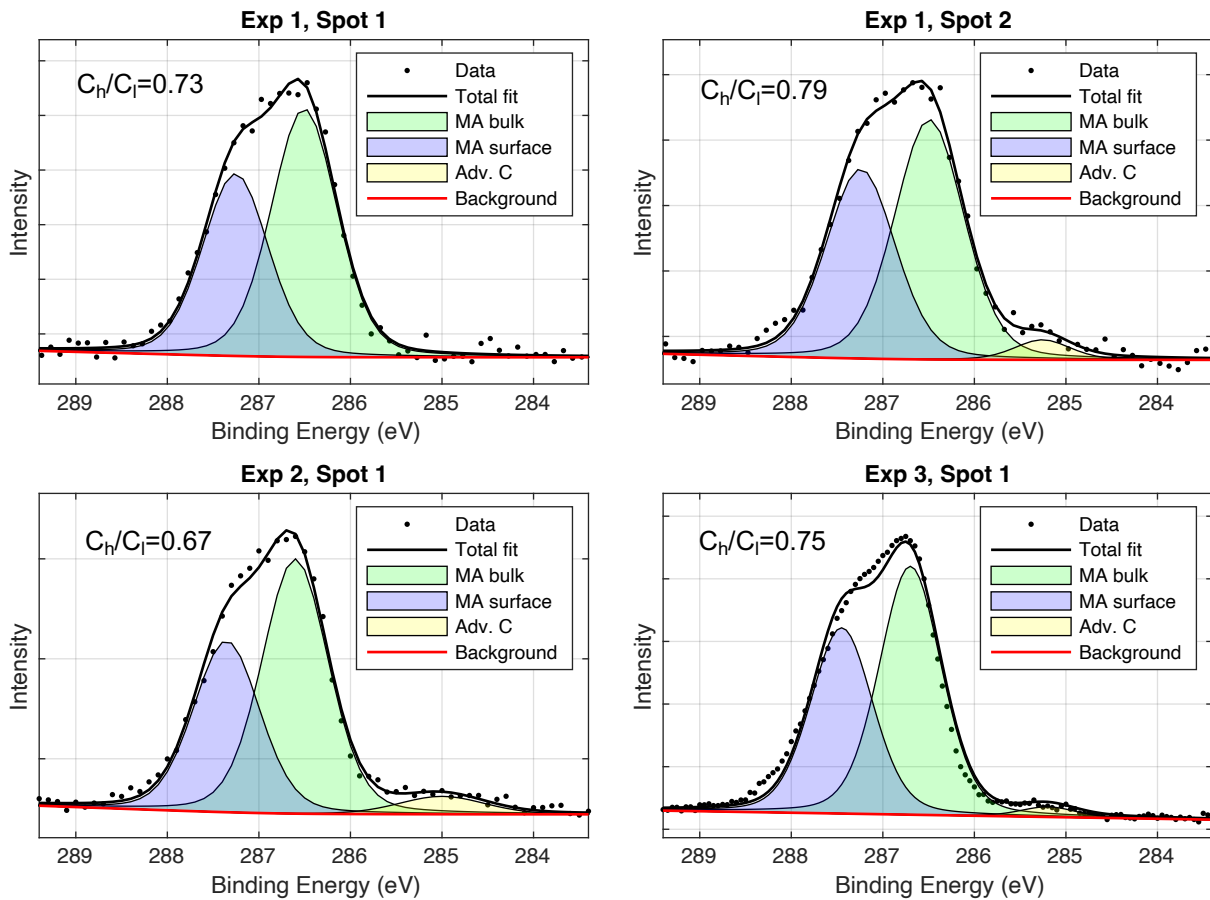


Figure S6: Curve fitting results of C 1s core level of  $\text{MAPbI}_3$  single crystal surfaces after cleaving recorded with a photon energy of 535 eV. Data for three different single crystals measured on three different occasions (Exp1, Exp2 and Exp3) and two different measurements spots on one of the single crystals (Spot1, Spot2) is shown. The intensity ratios of the MA surface contribution (blue,  $C_h$ ) and MA bulk contribution (green,  $C_l$ ) are given in the figures. The binding energy scale is calibrated versus the Fermi level through measurement of the Au 4f core level on a gold foil.

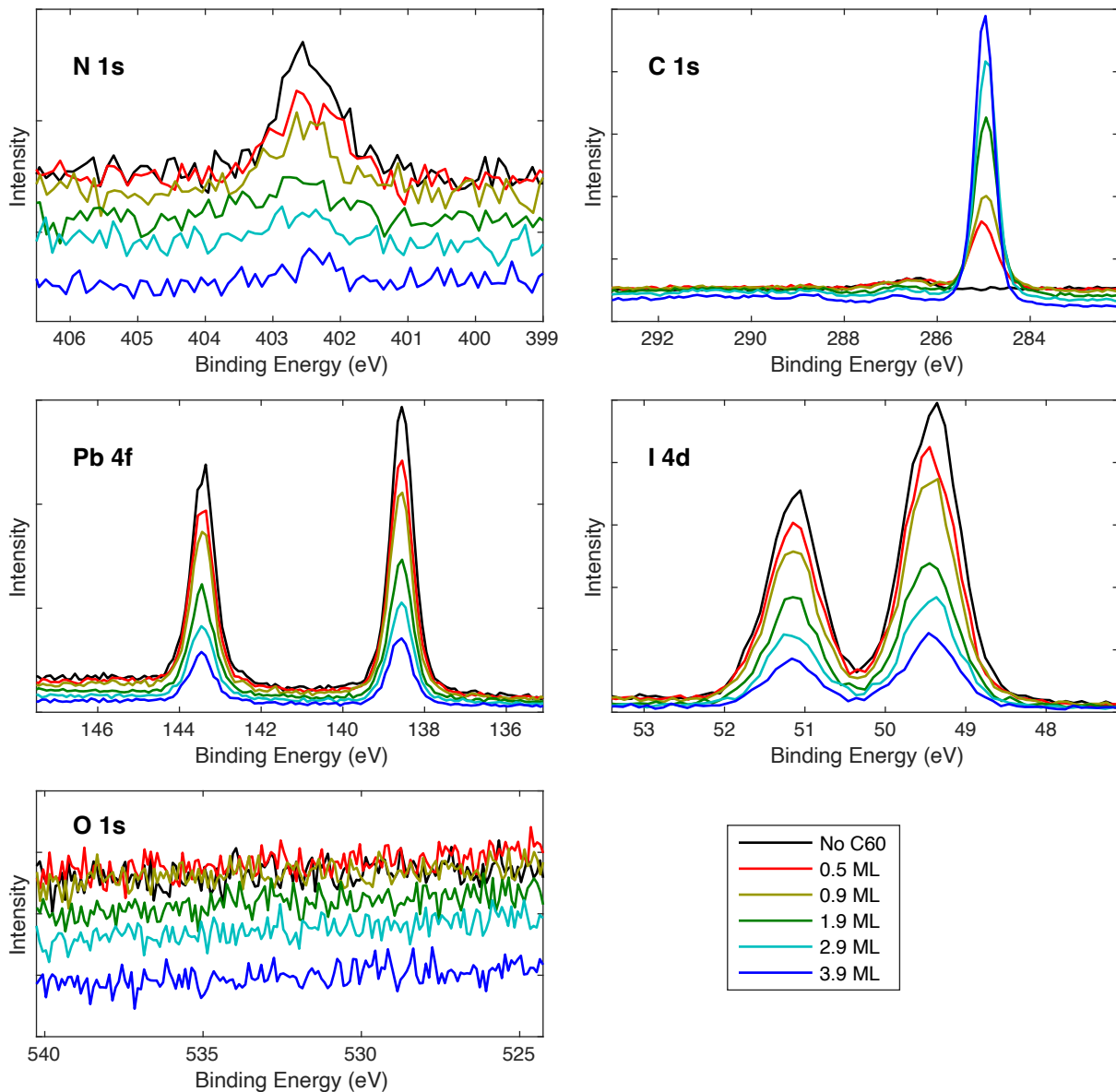


Figure S7. Core level spectra measured in Experiment 1, spot 1 after evaporation with an incident photon energy of 758 eV.

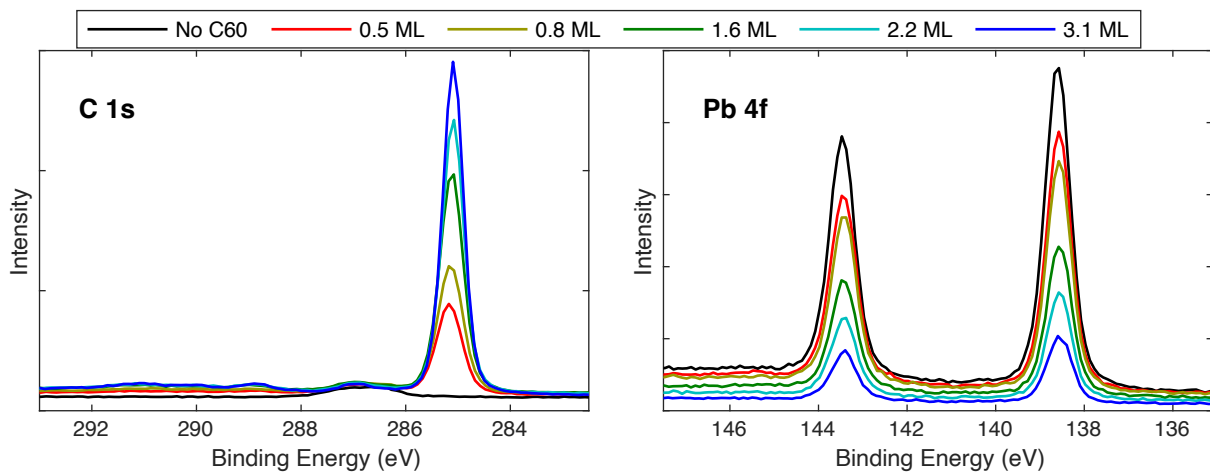


Figure S8. Core level spectra measured in Experiment 1, spot 2 after evaporation with an incident photon energy of 535 eV.

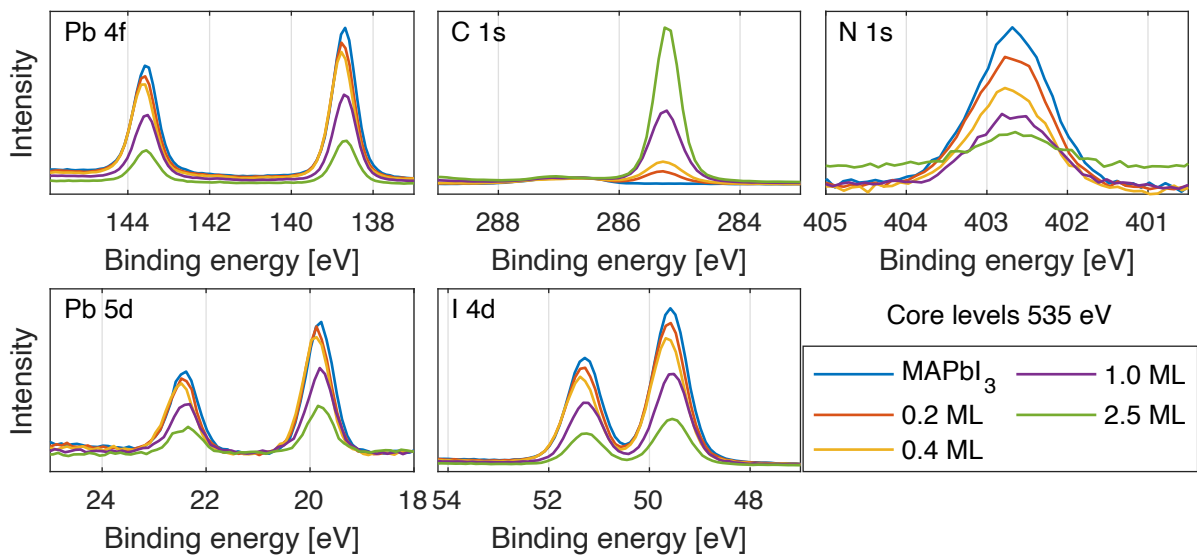


Figure S9. Core level spectra measured in Experiment 2, spot 1 after evaporation with an incident photon energy of 535 eV.

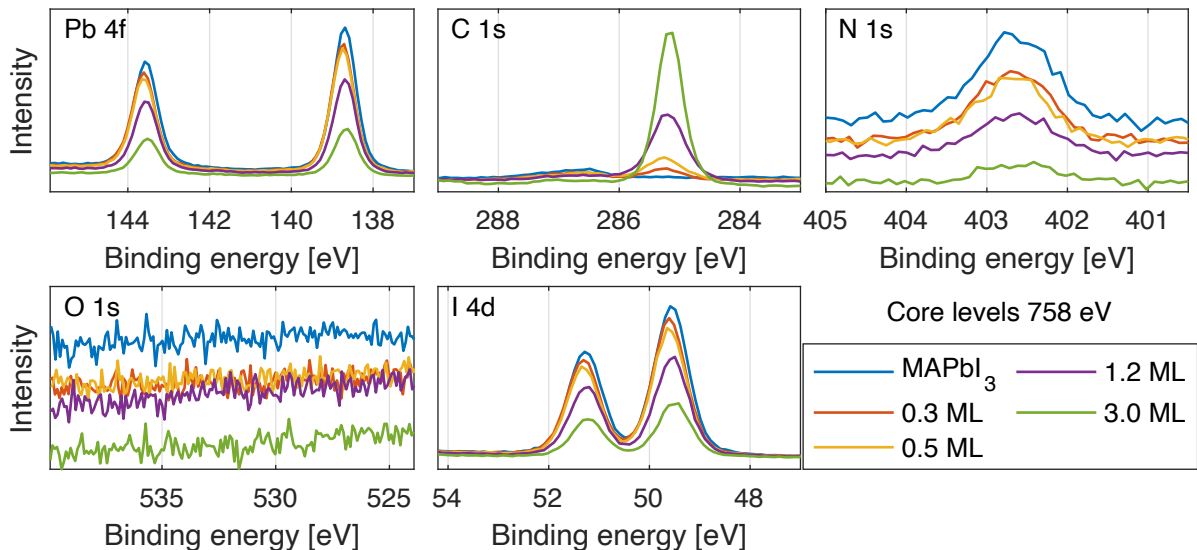


Figure S10. Core level spectra measured in Experiment 2, spot 1 after evaporation with an incident photon energy of 758 eV.

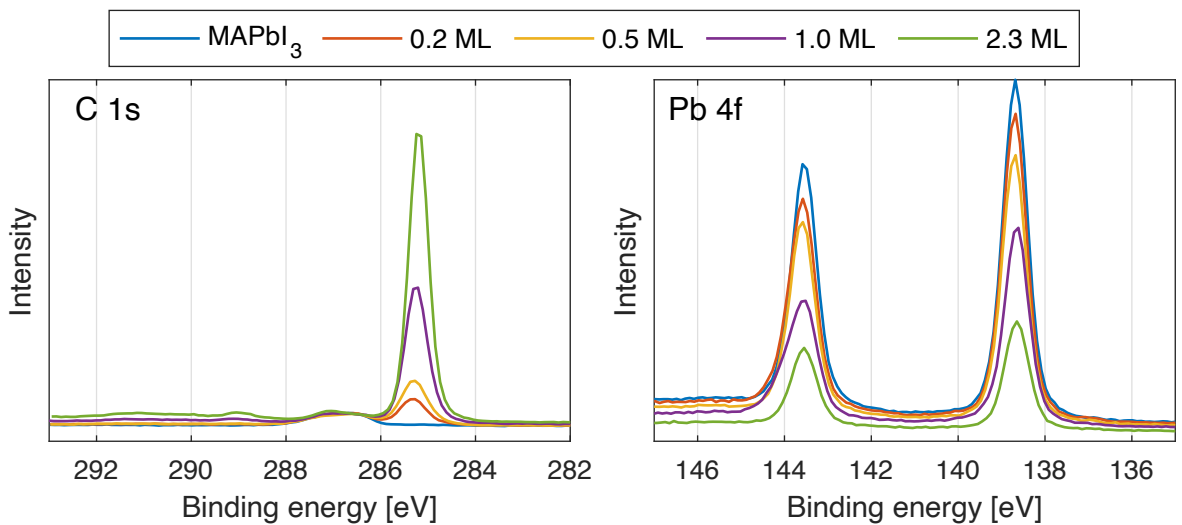


Figure S11. Core level spectra measured in Experiment 2, spot 2 after evaporation with an incident photon energy of 535 eV.

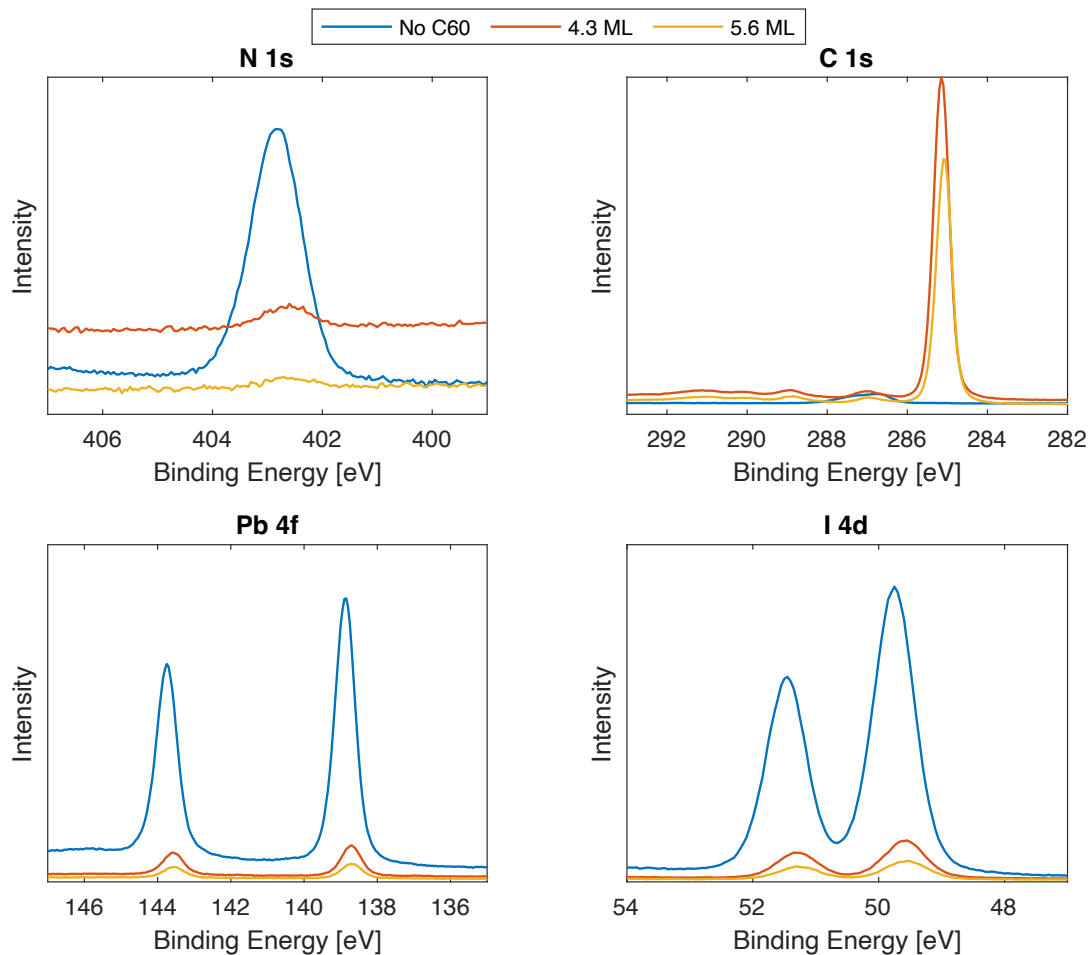


Figure S12. Core level spectra measured in Experiment 3, spot 1 after evaporation with an incident photon energy of 535 eV.

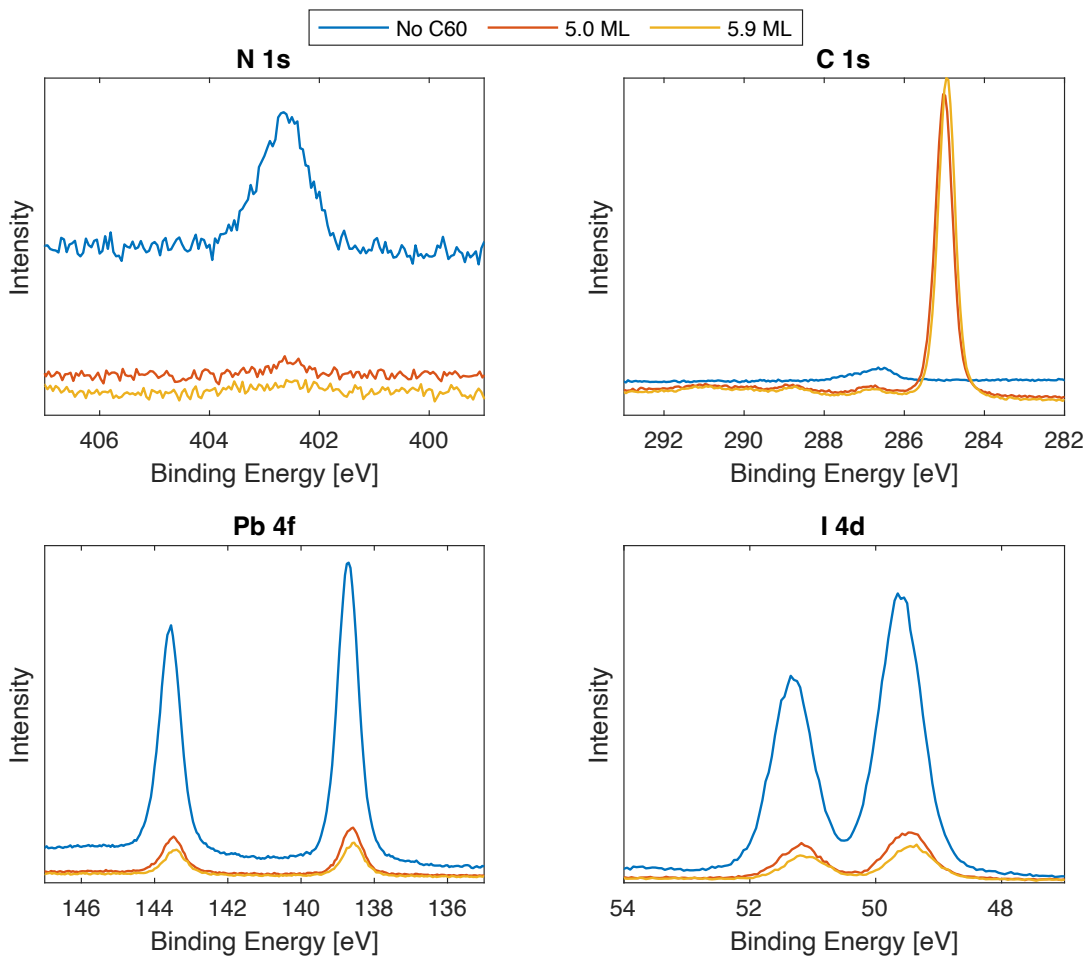


Figure S13. Core level spectra measured in Experiment 3, spot 1 with an incident photon energy of 758 eV.

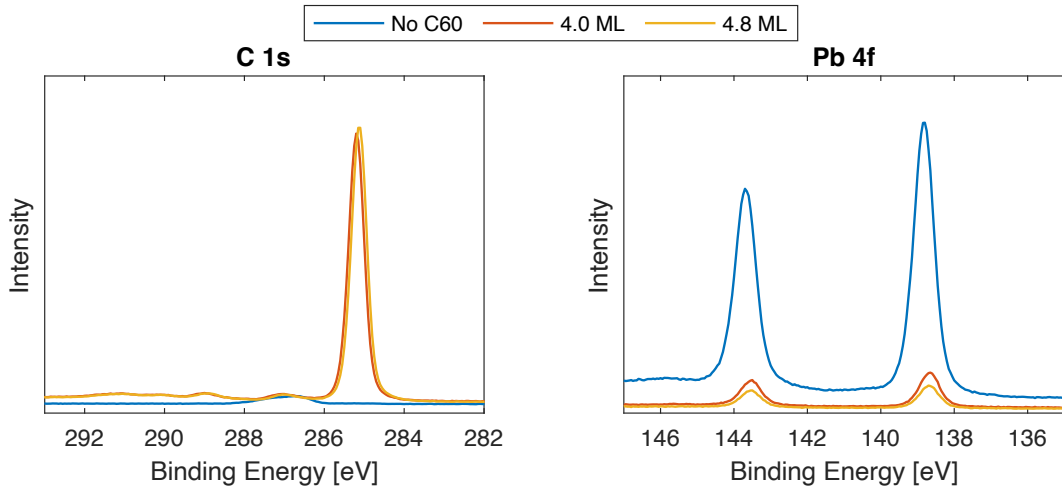


Figure S14. Core level spectra measured in Experiment 3, spot 2 with an incident photon energy of 535 eV.

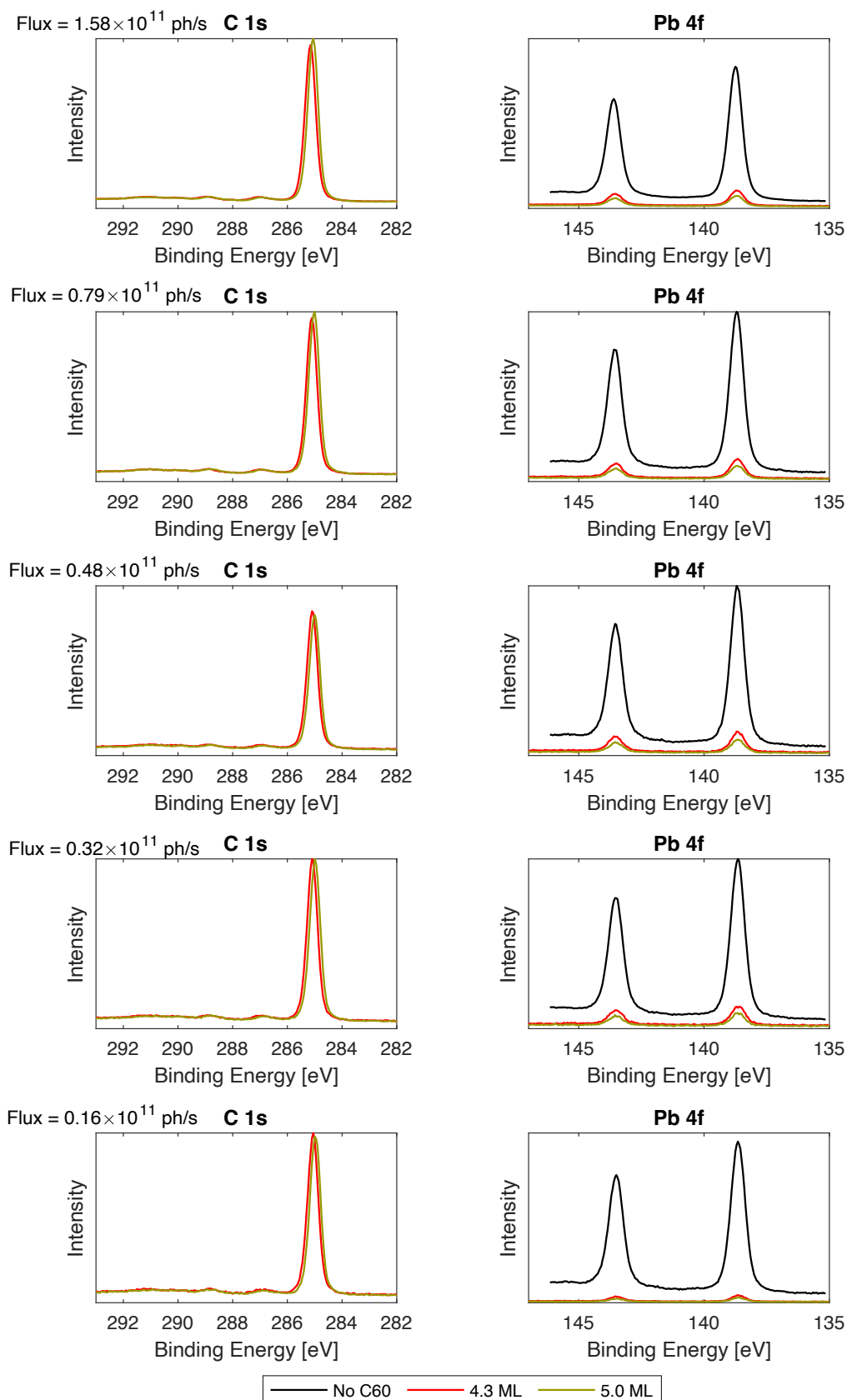


Figure S15. Core level spectra measured in Experiment 3, spot 3 at 535 eV incident photon energy with the photon flux density varied through adjusting the size of the exit slit.

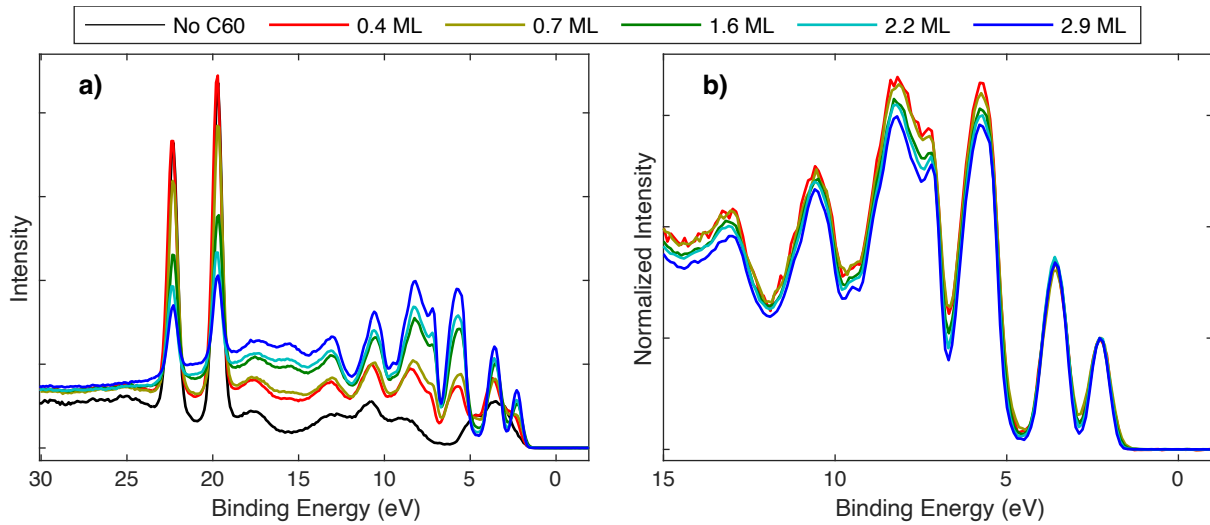


Figure S16: Core level spectra measured in Exp 1, spot 1 after evaporation with an incident photon energy of 758 eV. a) The spectra as measured energy calibrated to the Fermi level of a gold reference foil. b)  $C_{60}$ -only spectra obtained by subtracting the contribution of the perovskite from the spectra after  $C_{60}$  evaporation. These spectra are then energy aligned on the position of the HOMO peak of the  $C_{60}$  and normalized to this peak's maximum intensity.

#### Measurements at different photon flux values

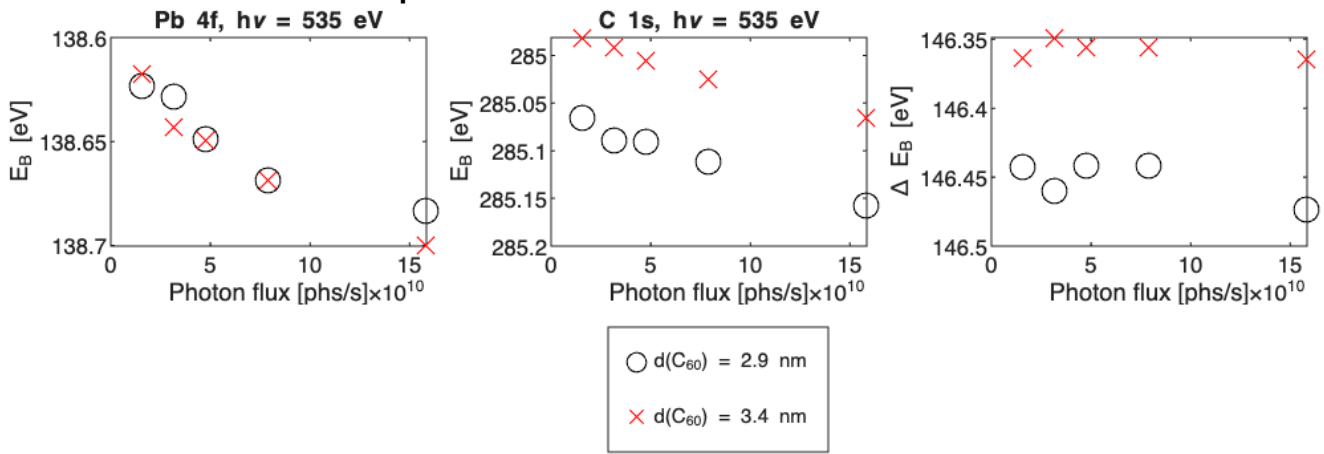


Figure S17 : Binding energy of the  $Pb\ 4f_{7/2}$  (left) and  $C\ 1s$  (middle) peak position and energy difference between the two (right) as a function of photon flux recorded in Exp3, spot 3, with 535 eV photon energy. The photon flux was varied by changing the size of the exit slit. The peak positions shift to higher binding energy with increasing photon flux, while the energy difference between them remains constant. This indicates reversible sample charging with higher X-ray intensities.

#### Energy difference between $Pb\ 4f_{7/2}$ peak and the $MAPbI_3$ valence band edge

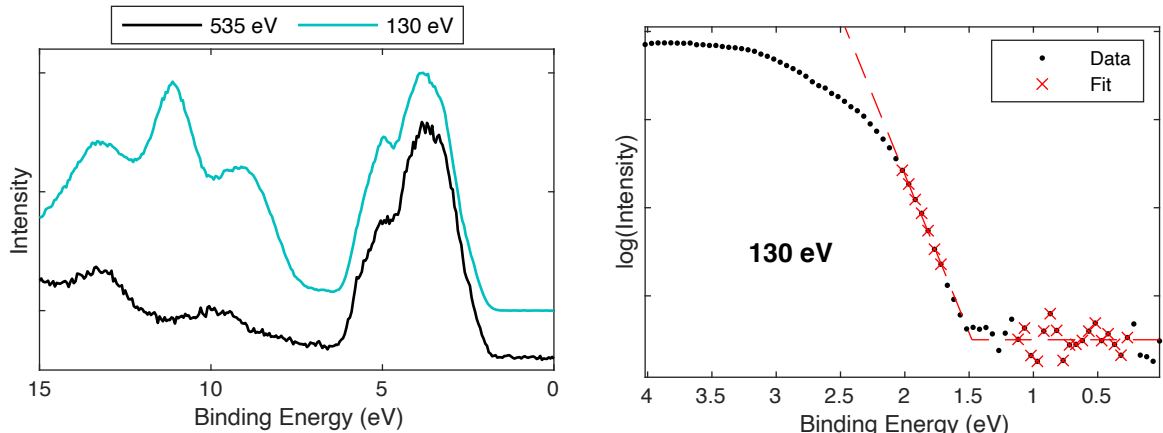


Figure S18: Left: Valence band spectra of MAPbI<sub>3</sub> crystal measured in Exp 3, spot 1 with 2 photon energies (130 eV and 535 eV) aligned to the Pb 5d<sub>5/2</sub> position at 20.01 eV recorded with a photon energy of 535 eV. Right: Valence band edge fit on a logarithmic axis to the data at 130 eV. The band edge was determined as the crossing point of the two fitted straight lines. The data at 130 eV was used due to the better signal-to-noise ratio at this photon energy.

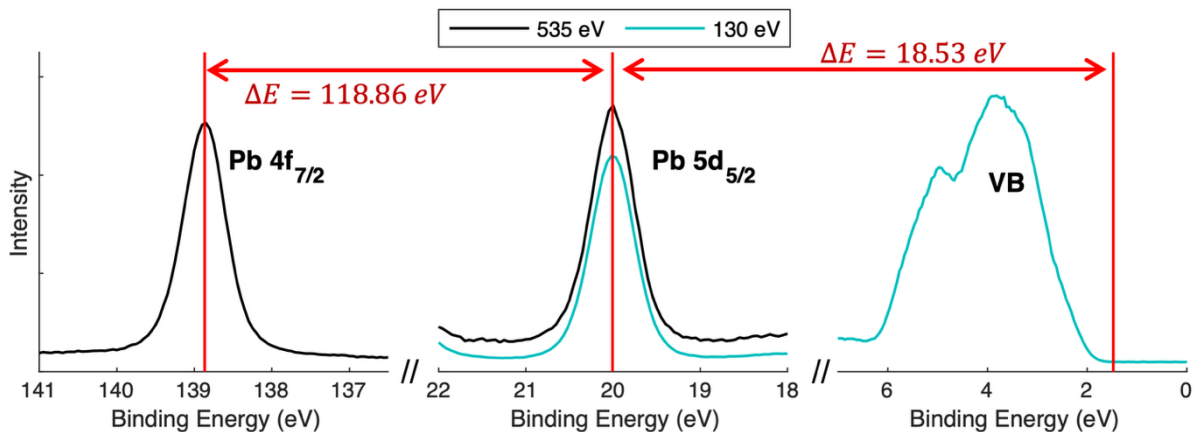


Figure S19: Spectra and positions recorded in Exp 3, spot 1 used for determining the energy offset between Pb 4f<sub>7/2</sub> and the valence band edge in MAPbI<sub>3</sub>. The energy difference between Pb 4f<sub>7/2</sub> and Pb 5d<sub>5/2</sub> (determined with a photon energy of 535 eV) was found to be 118.86 eV. The energy difference between Pb 5d<sub>5/2</sub> and the valence band edge (determined with a photon energy of 130 eV) was found to be 18.53 eV. This gives an energy difference between Pb 4f<sub>7/2</sub> and the valence band edge of 137.39 eV.

### Energy difference between C 1s peak and the C<sub>60</sub> HOMO edge

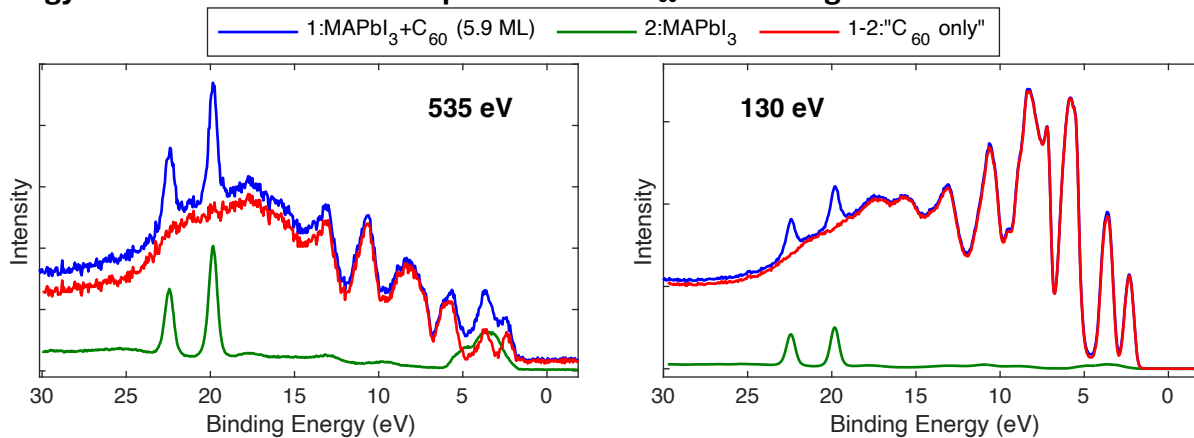


Figure S20: Valence band spectra of C<sub>60</sub> on MAPbI<sub>3</sub> crystal (5.9 ML) measured in Exp 3, spot 1 with two photon energies (535 eV, left and 130 eV, right) compared to spectra recorded on the clean MAPbI<sub>3</sub> surface in the same experiment. The MAPbI<sub>3</sub> spectra are calibrated and normalised to the Pb 5d intensity recorded in the spectra after evaporation. Using the two recorded spectra, C<sub>60</sub> only spectra are obtained by subtracting the MAPbI<sub>3</sub> contribution from the spectra after C<sub>60</sub> evaporation.

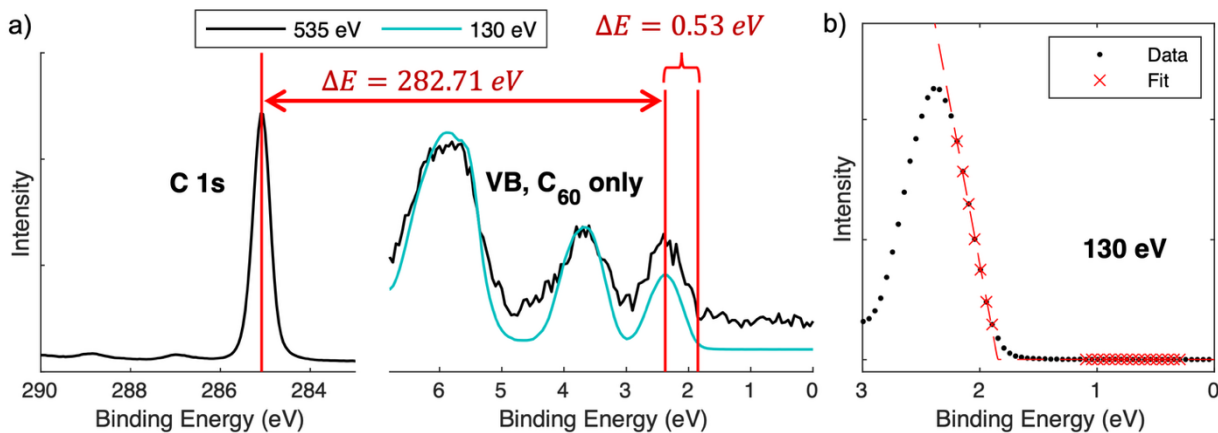


Figure S21: a) Spectra and positions recorded in Exp 3, spot 1 used for determining the energy offset between C 1s and the HOMO onset of C<sub>60</sub>. The valence band spectrum at 130 eV is energy calibrated to the spectrum at 535 eV by placing the HOMO peak position at the same energy. The energy difference between C 1s and the HOMO peak position (determined with a photon energy of 535 eV) was found to be 282.71 eV. The energy difference between the HOMO peak and the HOMO onset energy (determined with a photon energy of 130 eV) was found to be 0.53 eV. This gives an energy difference between C 1s and the HOMO onset of 283.24 eV. b) Linear fit to the HOMO edge of the C<sub>60</sub> only spectrum recorded at 130 eV and calibrated to the spectrum at 535 eV used to determine the HOMO onset energy indicated in (a).

## References

- (1) Rabenau, T.; Simon, A.; Kremer, R. K.; Sohmen, E. The Energy Gaps of Fullerene C<sub>60</sub> and C<sub>70</sub> Determined from the Temperature Dependent Microwave Conductivity. *Zeitschrift für Physik B Condensed Matter* 1993, 90 (1), 69–72.
- (2) Krätschmer, W.; Lamb, L. D.; Fostiropoulos, K.; Huffman, D. R. Solid C<sub>60</sub>: A New Form of Carbon. *Nature* 1990, 347 (6291), 354–358.
- (3) Liu, S.; Lu, Y.-J.; Kappes, M. M.; Ibers, J. A. The Structure of the C<sub>60</sub> Molecule: X-Ray Crystal Structure Determination of a Twin at 110 K. *Science* (1979) 1991, 254 (5030), 408–410. <https://doi.org/10.1126/science.254.5030.408>.
- (4) García-Fernández, A.; Svanström, S.; Sterling, C. M.; Gangan, A.; Erbing, A.; Kamal, C.; Sloboda, T.; Kammlander, B.; Man, G. J.; Rensmo, H.; Odelius, M.; Cappel, U. B. Experimental and Theoretical Core Level and Valence Band Analysis of Clean Perovskite Single Crystal Surfaces. *Small* 2022, 18 (13), 2106450. <https://doi.org/https://doi.org/10.1002/smll.202106450>.